Propagation in glass optical waveguides

R. Olshansky

Corning Glass Works, Research and Development Laboratory, Corning, New York

The propagation theory of multimode and single-mode optical waveguide fibers is reviewed. The subjects reviewed include basic propagation theory, the influence of the glass medium on attenuation and pulse dispersion, and the effects of perturbations of the waveguide's geometry and index profile.

CONTENTS

I. INTRODUCTION

Since the announcement by Corning Glass Works in 1970 of a 20 dB/km glass optical waveguide fiber (Kapron *et al.*, 1970), rapid advances have been made in the development of low-attenuation optical waveguides suitable for long-distance communications. The low attenuation, high information bandwidth and low projected manufacturing cost of glass waveguides make them an attractive alternative to the coaxial cables and multiple wire pair cables presently in use. The optical fiber's small size, low weight, and immunity to electromagnetic interference offer important additional benefits.

Following the development of laser and light-emitting-diode (LED) sources in the early 1960's, Kao and Hockham (1966) recognized that glass waveguides could be a practical transmission medium if transmission losses could be reduced to 20 dB/km by elimination of metallic impurities.

The vapor phase oxidation or chemical vapor deposition (CVD) technique has been spectacularly successful at achieving this. The vapors of high-purity liquids, such as $SiCl_4$ and $GeCl_4$, can be oxidized under controlled conditions to form a glass soot which is collected either on a rotating rod (Keck, Schultz, and Zimar, 1973) or on the inner surface of a tube (Keck and Schultz, 1973; MacChesney *et al.*, 1974). According to the method of soot collection, these are, respectively, referred to as either the outside or inside processes. Once the soot is deposited the resulting preform can be consolidated into glass and subsequently drawn into fiber.

The use of purified liquid reactants and the avoidance of conventional melting techniques can reduce contamination by metallic impurities to less than a few parts per billion (Maurer, 1973). By 1973 losses of 5 dB/km were being reported for a GeO_2–SiO_2 core, SiO_2 clad waveguide (Schultz, 1973; Keck, Maurer, and Schultz, 1973). At longer wavelengths where the intrinsic losses are lower, attenuation rates of 0.5 dB/km have recently been achieved in a P_2O_5–SiO_2 waveguide (Horiguchi and Osanai, 1976). The use of B_2O_3 (French *et al.*, 1973; Kato, 1973) and P_2O_5 (Payne and Gambling, 1974) as waveguide materials has increased the range of useful compositions.

A number of variations of the vapor phase deposition technique have been used successfully to make optical waveguides. For a comprehensive review of this subject see the paper by Schultz (1979).

Although the inside process was first conceived at Corning Glass Works (Keck and Schultz, 1973), it was actively pursued and more fully developed at Bell Telephone Laboratories (MacChesney *et al.*, 1974). The use, external to the collecting tube, of a traversing burner serves to initiate the reaction and consolidate the soot in a single step (MacChesney *et al.*, 1974). A further variation of the inside process using a plasma-activated reaction has also been demonstrated (Koenings *et al.*, 1975; Geittner *et al.*, 1976; Jaeger *et al.*, 1978).

Recently the outside process has been modified to achieve continuous preform fabrication by depositing soot on the end of a rotating silica rod (Izawa *et al.*, 1977). By means of such an axial deposition of soot, the soot can be deposited and then consolidated in a continuous process.

With the exception of the axial deposition, all these variations build a preform by depositing soot or glass in concentric layers. Since the composition can be varied from layer to layer, the process is well suited for fabricating fibers with precisely controlled graded-index profiles. This is an important advantage because the properly graded-index profile has an information bandwidth 10^2–10^3 greater than that of the ungraded profile.

An alternative to the vapor phase oxidation technique is the double crucible method (for a review see Newns *et al.*, 1977). Beginning with high-purity batch materials, the fiber is pulled continuously from a high-purity double platinum crucible. In 1974, much interest was generated when researchers (Koizumi *et al.*, 1974) at the Nippon Sheet Glass Company reported 20 dB/km parabolic index profile SELFOC fiber which had been fabricated by the double crucible process. The attainment of lower loss has proved to be difficult because of the requirement of very high-purity starting materials and the need to maintain purity during processing. Although losses as low as 5 dB/km have been achieved (Ikeda and Yoshiyagawa, 1976; Newns *et al.*, 1977), the difficulty of maintaining the highest purity levels and of accurately controlling the index profile puts the double crucible process at a disadvantage in the manufacture of low-attenuation, high-bandwidth fibers. In applications where the required fiber transmission properties are less severe the double crucible process may still be competitive.

Essential to the rapid progress in optical communication systems has been the simultaneous development of low-loss fibers and reliable, low-cost sources and detectors. While the subject of this review is the propagation characteristics of the optical waveguides, a brief survey of available sources and detectors seems appropriate for the reader who is not familiar with the field of optical communications.

The development of GaAs and GaAlAs LED's and injection lasers began in the early 1960's (for a review see Miller *et al.*, 1973). LED's with predicted lifetimes in excess of 10^7 h have been available for several years (Hersee and Goodfellow, 1976). Lifetimes of 10^6 h are now being predicted for injection lasers (Ladany *et al.*, 1977; Hartmann *et al.*, 1977). These sources operate in the spectral range 0.8–0.9 μm, where fiber attenuations of 3–5 dB/km are routinely achieved. Today GaAs and GaAlAs sources are used in almost all operating optical communication systems and field trials.

The attenuation of optical fiber decreases to 0.5-1 dB/km in the 1.0–1.5 μm spectral range. The severalfold increase in repeater spacing made possible by such low attenuation makes optical communications at these wavelengths even more attractive. An additional attraction of the longer wavelengths is a first-order zero in the material-related pulse dispersion occurring near 1.3 μm. Transmission at this wavelength leads to a potential increase in the information bandwidth by one to two orders of magnitude.

Results have been reported on the recent development of GaInAsP/InP lasers (Shen *et al.*, 1977) and LED's (Gibbons, 1977) which operate at these longer wavelengths. These devices appear to be very promising and are expected to be commercially available in the near future.

In the region 0.8–0.9 μm, silicon avalanche photodiodes (APD's) and silicon p–i–n photodiodes are available for optical communication systems (for a review see Misugi and Takanashi, 1977). At wavelengths greater than 1.1 μm, where the Si detectors cut off, Ge APD's can be used. Because of excess noise, at a fixed bit-error rate they are about 10 dB less sensitive than the Si APD's. Gallium–indium–arsenide–phosphide alloys are also being studied for use in the longer-wavelength region. An excellent review has been given by Pearsall (1978).

For an up-to-date survey of sources, detectors, and optical systems design, the reader is referred to the review by Conradi *et al.* (1978).

This paper follows a number of excellent review articles. Maurer (1973) discussed the properties of the glass medium, while the article by Miller *et al.* (1973) deals in detail with propagation in optical fibers, devices, and systems considerations. Gloge (1975a) has provided an excellent review of waveguide propagation theory.

In addition to these references, there are several textbooks available which offer an introduction to optical waveguide theory (Kapany and Burke, 1972; Marcuse, 1972c, 1974a; Arnaud, 1976b; Unger, 1977).

Since the publication of these reviews and texts, considerable progress has been made in the understanding of waveguide propagation, particularly in understanding the influence of the glass medium on propagation characteristics. Thus, many new developments, not previously reviewed, are included here.

Section II. of this article reviews the propagation characteristics of the unperturbed multimode optical fiber assuming an ideal, lossless, dispersionless dielectric medium. Section III considers the very important effects that the glass medium has on waveguide propagation, and Sec. IV deals with deviations from the ideal multimode waveguide geometry, such as curvature of the waveguide, the finite cladding thickness, and perturbations. The final section reviews the properties of the single-mode waveguide.

II. THE MULTIMODE OPTICAL WAVEGUIDE

A fiber optical waveguide consists of a cylindrically symmetric core region surrounded by a cladding region. If the refractive index of the core is greater than that of the cladding, light is guided along the waveguide core. The ideal waveguide is straight, cylindrically symmetric, has a cladding of infinite thickness, and is made of a lossless, dispersionless dielectric material. The theory of the ideal unperturbed multimode waveguide is reviewed in this section.

The core of radius a is taken to lie along the positive z axis with input end at the origin. A cylindrically symmetric, but otherwise arbitrary, refractive index profile can be defined by the expression

$$n^2(r) = n_1^2[1 - 2\Delta f(r/a)], \quad r \leqslant a,$$
$$n^2(r) = n_2^2 = n_1^2[1 - 2\Delta f(1)], \quad r \geqslant a, \tag{2.1}$$

where the profile function $f(r/a)$ is normalized so that

$$f(0) = 0,$$
$$f(1) = 1. \tag{2.2}$$

The refractive index along the waveguide's axis is n_1 and the index of the cladding is n_2. The quantity Δ is defined as

$$\Delta = (n_1^2 - n_2^2)/(2n_1^2). \tag{2.3}$$

For optical waveguides used for telecommunication, the difference between n_1 and n_2 is on the order of 10^{-2}. Thus,

$$\Delta \approx (n_1 - n_2)/n_1, \tag{2.4}$$

and Δ is referred to as the relative index difference.

For waves with free-space wavelength λ propagating in the positive z direction, the electromagnetic fields can be written as

$$\overline{E}(r, \theta, z, t) = \overline{E}(r, \theta)e^{i(\beta z - \omega t)},$$
$$\overline{H}(r, \theta, z, t) = \overline{H}(r, \theta)e^{i(\beta z - \omega t)}, \tag{2.5}$$

where β is the propagation constant and ω is the angular frequency ($\omega = 2\pi f$). Maxwell's equations for the optical waveguide can be written as (see Born and Wolf, 1970)

$$[\nabla_T^2 - \beta^2 + k^2n^2(r)]\overline{E}(r, \theta) + \overline{\nabla}\{\overline{E} \cdot \overline{\nabla} \log[n^2(r)/\mu_0]\} = 0, \tag{2.6}$$

$$[\nabla_T^2 - \beta^2 + k^2n^2(r)]\overline{H}(r, \theta) + \overline{\nabla}\{\log[n^2(r)/\mu_0]\} \times \operatorname{curl}\overline{H}(r, \theta) = 0, \tag{2.7}$$

where $k = 2\pi/\lambda$ is the free-space wave number and ∇_T is the transverse gradient operator.

The propagation constant β, introduced in Eq. (2.5) is very important for characterizing solutions to the wave equation. For real β, two classes of solutions exist (Snitzer, 1961). For β in the range

$$n_1k \geqslant |\beta| \geqslant n_2k, \tag{2.8}$$

propagating electromagnetic fields exist only within the core region, and these solutions decrease exponentially in the cladding. For this class of solutions, one is led to an eigenvalue equation and a finite number of guided mode solutions.

If β is real and in the range

$$n_2k > \beta > -n_2k, \tag{2.9}$$

waves can fully propagate in both core and cladding, and a continuum of solutions exist. These are referred to as the radiation modes or continuum solutions.

There is also a third class of modes (Snyder and Mitchell, 1974; Snyder *et al.*, 1974), called leaky modes, which can be characterized by the conditions

$$\operatorname{Im}\beta > 0 \tag{2.10}$$

and

$$n_2k > \operatorname{Re}\beta > -n_2k. \tag{2.11}$$

The leaky modes are in many ways analogous to the well-known resonant states of quantum mechanics. Their power is only temporarily confined within the core region of the waveguide.

In analyzing guided mode propagation, it is convenient to introduce parameters U, W, and V by the equations (Snyder, 1969),

$$U = a(n_1^2k^2 - \beta^2)^{1/2}, \tag{2.12}$$

$$W = a(\beta^2 - n_2^2k^2)^{1/2}, \tag{2.13}$$

$$V = (U^2 + W^2)^{1/2}. \tag{2.14}$$

Together these three equations define V in terms of the waveguide parameters,

$$V = n_1ka\sqrt{2\Delta}. \tag{2.15}$$

Later discussion will make it clear that V provides a measure of the waveguide's mode volume.

For the special case of a step-index waveguide having a uniform core of index n_1, $f(r)$ is identically zero and Eqs. (2.6) and (2.7) reduce to

$$[\nabla_T^2 + k^2n^2(r) - \beta^2]\overline{E}(r, \theta) = 0,$$
$$[\nabla_T^2 + k^2n^2(r) - \beta^2]\overline{H}(r, \theta) = 0. \tag{2.16}$$

Exact solutions (Snitzer, 1961) to Eq. (2.16) are known. The exact eigenvalue equation and the field solutions are very complicated, and it is difficult to use them to gain physical insight into waveguide propagation. For a discussion of the exact solution, the reader is referred to either the original paper by Snitzer (1961) or to one of the available texts (Marcuse, 1972c, 1974a) on the subject.

A. Weak guidance approximation

Optical waveguides used for telecommunications have small relative index difference. A Δ of about 0.035 is the largest value yet reported (O'Connor *et al.*, 1977), but Δ values in the range 0.01–0.02 are more typical. For such small index differences, the "weak guidance" approximation (Snyder, 1969; Gloge, 1971a) leads to simplified solutions of the wave equation which prove to be extremely useful. The following discussion of the weak guidance approximation is based on the work of Gloge (1971a, 1975a).

In the weak guidance approximation, the transverse fields are assumed to have the form

$$E_y(r, \theta) = H_x\begin{Bmatrix} \varepsilon_0\mu_0/n_1 \\ \varepsilon_0\mu_0/n_2 \end{Bmatrix} = E_y(a)\begin{Bmatrix} \dfrac{J_\nu(Ur/a)}{J_\nu(U)} \\ \dfrac{K_\nu(Wr/a)}{K_\nu(W)} \end{Bmatrix}\cos(\nu\theta), \tag{2.17}$$

where the upper and lower equations are for core and cladding, respectively. ν is a non-negative integer referred to as the azimuthal or angular mode number.

Longitudinal fields, E_z and H_z, can be calculated from the derivatives of the transverse fields. They are reduced in amplitude relative to the transverse fields by a factor of order $\Delta^{1/2}$. Differentiations of the longitudinal fields to regenerate the transverse fields lead to fields which differ from the originals by order Δ. Thus the assumed fields of Eq. (2.17) satisfy Maxwell's equation to within correction terms of order Δ.

Equation (2.17) must also satisfy continuity conditions at the core–cladding interface. To order Δ, n_1 is equal to n_2, so that in the weak guidance approximation the boundary condition requires continuity of the fields and their derivatives. This gives the eigenvalue condition

$$U\frac{J_\nu'(U)}{J_\nu(U)}=W\frac{K_\nu'(W)}{K_\nu(W)}\,. \tag{2.18}$$

Using the recurrence relation for Bessel functions, the eigenvalue equation (2.18) can be written as either

$$U\frac{J_{\nu-1}(U)}{J_\nu(U)}=-W\frac{K_{\nu-1}(W)}{K_\nu(W)} \tag{2.19a}$$

or

$$U\frac{J_{\nu+1}(U)}{J_\nu(U)}=W\frac{K_{\nu+1}(W)}{K_\nu(W)}\,. \tag{2.19b}$$

Gloge has shown that these simplified equations can be derived directly for the exact eigenvalue equation.

In Eq. (2.17) the orthogonal orientation, with angular dependence $\sin(\nu\theta)$ instead of $\cos(\nu\theta)$, is an independent solution, as is the orthogonal polarization, with x and y interchanged. Thus if $\nu=0$, there are two independent solutions, and if $\nu\neq 0$, there are four.

Before discussing the solution to the eigenvalue condition, it is interesting to consider the physical interpretation of the weak guidance approximation.

Equation (2.16) is formally identical to the Klein–Gordon equation describing the quantum-mechanical wave function of a massless, scalar (spin zero) field propagating in a potential. Using the well-known relations for the momentum operator in quantum mechanics,

$$\bar{p}=\frac{\hbar}{i}\bar{\nabla}\,, \tag{2.20}$$

and for the energy operator,

$$E=-\frac{\hbar}{ic}\frac{\partial}{\partial t}\,. \tag{2.21}$$

The approximate wave equation (2.16) can be written as

$$[E^2-p^2-V(r)]\begin{Bmatrix}\bar{E}\\ \bar{H}\end{Bmatrix}=0\,, \tag{2.22}$$

where the potential is defined as

$$V(r)=-\hbar^2k^2[n^2(r)-n_1^2]\,. \tag{2.23}$$

Equations (2.22) and (2.23) show that in the weak guidance approximation Maxwell's equations are equivalent to the field equation of a scalar particle freely propagating along the waveguide's axis and confined by a potential in the transverse directions.

The neglect of the field's polarization implicit in Eqs. (2.16) and (2.22) can be understood as a consequence of the small grazing angle the guided waves make at the core–cladding interface. For total internal reflection at the interface the grazing angle θ must be in the range $0\leqslant\theta\leqslant(2\Delta)^{1/2}$. The Fresnel reflection formulas show that reflections are independent of polarization to order Δ. Hence in the weak guidance approximation the photon's polarization can be neglected.

B. Step-index profile

The number of modal solutions of Eq. (2.19a) can be determined as follows. Since W and $K_\nu(W)$ are positive, the right-hand side of Eq. (2.19a) is always negative. As a result of the oscillatory nature of the J_ν Bessel functions of positive argument, the left-hand side of the eigenvalue equation oscillates between $-\infty$ and $+\infty$, in much the same way as the tangent functions. In fact for large U one has

$$U\frac{J_{\nu-1}(U)}{J_\nu(U)}\approx -U\tan\left(U-\frac{\nu\pi}{2}-\frac{\pi}{4}\right)\,. \tag{2.24}$$

Since β lies in the interval given by Eq. (2.8), from the definition of U, one has

$$0\leqslant U\leqslant V\,. \tag{2.25}$$

Between each zero of $J_{\nu-1}(U)$ in this domain, there is a solution. Successive solutions will be labeled by the non-negative integer μ, which is referred to as the radial mode number. Designating the successive zeros of $J_{\nu-1}(U)$ by $Z_{\nu\mu}$ and the successive solutions by $U_{\nu\mu}$, one thus has

$$0<U_{\nu 0}\leqslant Z_{\nu 0}<U_{\nu 1}<Z_{\nu 1}\cdots Z_{\nu n-1}<U_{\nu n}\leqslant V\,. \tag{2.26}$$

Gloge (1971a) has introduced the label $LP_{\nu,\mu+1}$ to designate these linearly polarized solutions. Each $LP_{\nu,\mu+1}$ mode is a superposition of two of the exact modal solutions which are approximately degenerate.

For modes with large radial mode number

$$Z_{\nu\mu}\approx(\mu+\tfrac{1}{2}\nu+\tfrac{3}{4})\pi\,, \tag{2.27}$$

and one has the approximate restriction on mode number

$$2\mu+\nu\leqslant 2V/\pi\,. \tag{2.28}$$

Equation (2.28) is valid for waveguides with large V values.

Counting both angular orientations and both polarizations, the total number of modes N of the step waveguide is approximately given as (Gloge, 1971a)

$$N\approx\frac{4}{\pi^2}V^2\approx\frac{1}{2}V^2\,. \tag{2.29}$$

The power density in a mode is given as (Gloge, 1971a)

$$p(r,\theta)=\kappa_\nu\frac{U^2}{V^2}\frac{2P}{\pi a^2}\begin{Bmatrix}\dfrac{J_\nu^2(Ur/a)}{J_\nu^2(U)}\\[2mm] \dfrac{K_\nu^2(Wr/a)}{K_\nu^2(W)}\end{Bmatrix}\cos^2(\nu\theta)\,, \tag{2.30}$$

where

$$\kappa_\nu=K_\nu^2(W)/K_{\nu-1}(W)K_{\nu+1}(W) \tag{2.31}$$

and P is the total power per unit length. The power distribution given by Eq. (2.30) is the near-field intensity pattern of a mode and can be directly observed if an individual mode is excited. From Eq. (2.30) it is clear that the near-field pattern of mode μ,ν is characterized by μ radial nodes of zero intensity, corresponding to the zeros of $J_\nu^2(Ur/a)$, and 2ν azimuthal nodes corresponding to the zeros of $\cos^2(\nu\theta)$.

By integrating Eq. (2.30), one finds the power fraction in the cladding to be (Gloge, 1971a)

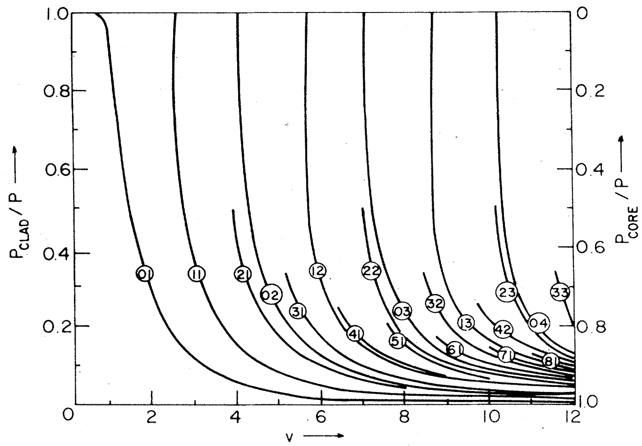

FIG. 1. The fraction of guided mode power in the cladding of a step-index wave guide is plotted vs the waveguide's V value (after Gloge, 1971a).

$$P_{clad}/P=(U^2/V^2)(1-\kappa_\nu). \tag{2.32}$$

This function is plotted in Fig. 1 for some of the low-order modes. As V increases, each mode becomes more strongly confined to the core and the fraction of power in the cladding approaches zero.

The modal propagation constants are of great importance in calculating modal group velocities and for analyzing the effects of perturbations. Solutions obtained from Eq. (2.19) are shown in Fig. 2 as a function of the parameter b, defined as (Gloge, 1971a)

$$b=1-\left(\frac{U}{V}\right)^2=\frac{(\beta^2-m_2^2k^2)}{2m_1^2k^2\Delta} \tag{2.33}$$

Various approximations for calculating b can be found in the literature (Marcuse, 1972c, 1974a). From Fig. 2, it can be seen that the region of single-mode propagation (LP_{01} or HE_{11} mode) occurs for $V\leq 2.405$. Single-mode waveguides are discussed in detail in Sec. V.

As V increases, b increases for each mode, eventually approaching the limit $b=1$ where the propagation constant $\beta\approx n_1k$. As V decreases, b decreases for each mode until it reaches the cutoff point where $b=0$ and $\beta=n_2k$.

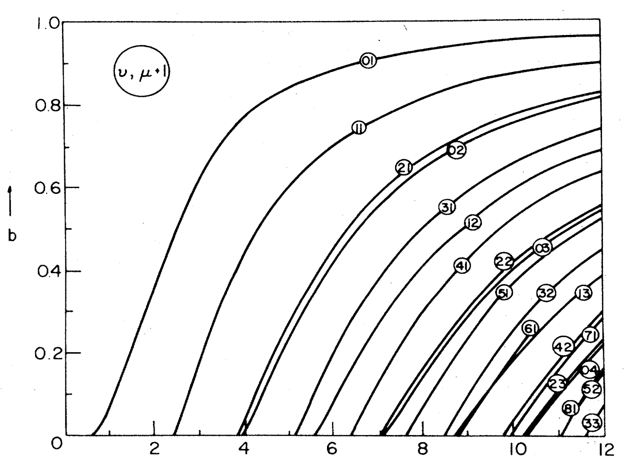

FIG. 2. The propagation parameter b is shown as a function of V for some of the lower-order modes of a step-index waveguide.

C. Parabolic-index profile

Optical waveguides with parabolic- or nearly parabolic-index profiles have transmission bandwidths which are orders of magnitude greater than those of step-index waveguides (Miller, 1965; Kawakami and Nishizawa, 1968; Uchida *et al.*, 1970) and play a central role in long-distance optical communication. The parabolic profile is defined as

$$\begin{aligned} n^2(r)&=n_1^2[1-2\Delta(r/a)^2], \quad r\leq a,\\ n^2(r)&=n_1^2[1-2\Delta]=n_2^2, \quad r\geq a. \end{aligned} \tag{2.34}$$

Exact solutions of the scalar wave equation,

$$\left[\frac{1}{r}\frac{d}{dr}r\frac{d}{dr}-\frac{\nu^2}{r^2}+k^2n_1^2-\beta^2-\left(\frac{V}{a}\right)^2\left(\frac{r}{a}\right)^2\right]E(r)=0, \tag{2.35}$$

are given as (Olshansky, 1976a)

$$E(r)=Ne^{-\rho/2}\rho^{\nu/2}L_\mu^\nu(\rho), \tag{2.36}$$

where

$$\rho=V(r/a)^2, \tag{2.37}$$

and $L_\mu^\nu(\rho)$ is the generalized Laguerre polynomial. The normalization factor N is defined as

$$N=2V(\mu!/(\mu+\nu)!)^{1/2}, \tag{2.38}$$

so that

$$1=\int_0^\infty E^2(r)\frac{r\,dr}{a^2}. \tag{2.39}$$

The propagation constant of the parabolic profile is

$$\beta=n_1k[1-4\Delta(2\mu+\nu+1)/V)]^{1/2}. \tag{2.40}$$

The field solutions given above are useful for analyzing propagation in waveguides with parabolic-index profiles, and, as discussed in Sec. IV, for analyzing the effects of index profile perturbations.

The solutions given by Eq. (2.36) are based on the implicit assumption that the parabolic profile extends to infinity. As a result, these solutions become inaccurate for the highest-order modes having β nearly equal to n_2k (Hashimoto, 1976; Okamoto and Okoshi, 1976).

D. WKB approximation

For multimode waveguides, the WKB method yields simple and useful approximations for the propagation constants of graded-index waveguides. The mathematical details of the technique and the approximate solution for the fields are discussed in the Appendix. The resulting eigenvalue equation is (Gloge and Marcatili, 1973)

$$\left(\mu+\frac{1}{2}\right)\pi=\int_{r_1}^{r_2}dr\,q(r), \tag{2.41}$$

where

$$q(r)=\sqrt{k^2n^2(r)-\beta^2-\nu^2/r^2}. \tag{2.42}$$

r_1 and r_2 are the positive, real zeros of $q(r)$ and are re-

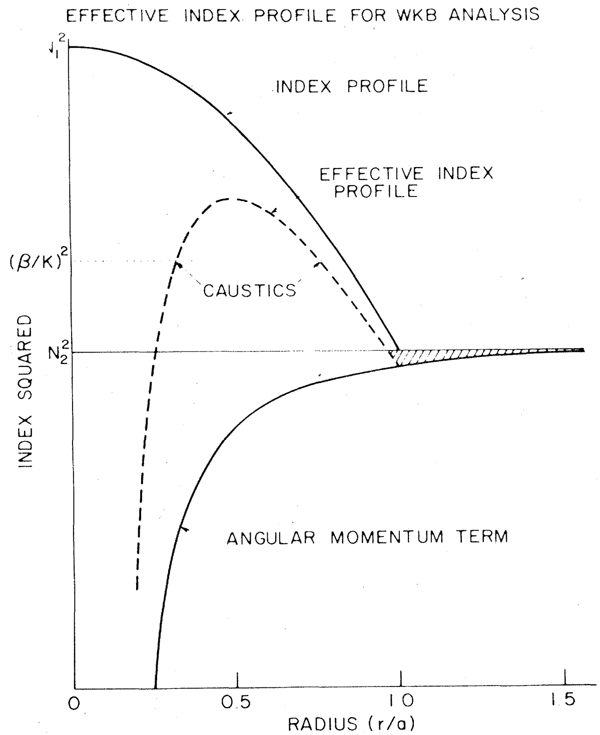

FIG. 3. The effective index profile (dashed curve) is the sum of the actual index profile and angular momentum term. The caustics for a mode with propagation constant β are indicated.

ferred to as either caustics or classical turning points.

The location of the caustics for a typical graded-index profile is illustrated in Fig. 3. The combination of the index profile term and the angular momentum term form an effective index profile shown by the dashed line, and defined as

$$n_{\mathrm{eff}}^2(r) = n^2(r) - \nu^2/(kr)^2 . \tag{2.43}$$

Most of the power in mode μ, ν is confined between the caustics at r_1 and r_2. For $r \leqslant r_1$, the power decreases as $(r/a)^\nu$, while for $r \geqslant r_2$ the power falls exponentially, as given by the WKB eigenfunction of the Appendix.

The integration of Eq. (2.41) can be performed explicitly only for step-index and parabolic index profiles.

Gloge and Marcatili (1973) have considered the special class of power-law or α-class index profile defined by

$$n^2(r) = n_1^2[1 - 2\Delta(r/a)^\alpha] . \tag{2.44}$$

For this class of profiles, it is possible to introduce a mode-ordering number n which enumerates the modes in order of decreasing propagation constant, that is,

$$n_1 k \geqslant \beta_1 \geqslant \beta_2 \geqslant \beta_3 \cdots > \beta_n > n_2 k . \tag{2.45}$$

They have found the solution

$$\beta = n_1 k[1 - 2\Delta(n/N)^{\alpha/(\alpha+2)}]^{1/2} , \tag{2.46}$$

where the total number of modes N is

$$N = \frac{\alpha}{\alpha+2} n_1^2 k^2 a^2 \Delta . \tag{2.47}$$

A modification of the familiar WKB method, developed explicitly for cylindrical geometry, had earlier been applied by Streifer and Kurtz (1967) to study the α-class of profiles. This method, developed by Langer (1949) and McKelvey (1959), approximates solutions to the cylindrical radial wave equation by Bessel functions having modified arguments. It is completely analogous to the normal WKB approach which approximates field solutions by sines and cosines having modified arguments. The Langer–McKelvey method offers the advantage that the inner turning point, resulting from the angular momentum term, is automatically taken into account by use of the J_ν Bessel function.

The resulting eigenvalue equation is (Streifer and Kurtz, 1967)

$$(2\mu + \nu + 1)\frac{\pi}{2} = \int_0^{r_0} dr \sqrt{k^2 n^2(r) - \beta^2} , \tag{2.48}$$

where r_0 is the solution of

$$kn(r_0) = \beta . \tag{2.49}$$

For power-law profiles, Eq. (2.48) has the solution

$$\beta = n_1 k[1 - 2\Delta(m/M)^{2\alpha/(\alpha+2)}]^{1/2} , \tag{2.50}$$

where

$$m = 2\mu + \nu + 1 \tag{2.51}$$

and

$$M^2 \approx \frac{\alpha}{\alpha+2}(n_1 k a)^2 \Delta . \tag{2.52}$$

The mode number m defined by Eq. (2.51) is called the principal mode number or mode group number. Equations (2.50) and (2.51) show that the degeneracy in propagation constant found in Eq. (2.40) for the parabolic index profile ($\alpha = 2$) is approximately valid for all power-law profiles. In fact, Eq. (2.48) shows that this degeneracy is approximately valid for all cylindrically symmetric profiles.

The Streifer–Kurtz solutions are in close agreement with the Gloge–Marcatili solutions provided one makes the identification

$$m = \sqrt{n} , \quad M = \sqrt{N} , \tag{2.53}$$

between the principal mode number m and the mode-ordering number n.

For $\alpha = 2$, these two methods give propagation constants which are identical to the Laguerre–Gauss solutions. For nearly parabolic profiles ($\alpha \approx 2$), the error of either method is expected to be small. Although an exact analysis of the errors has not been made, differences between the WKB method and the Langer–McKelvey method are expected to be of the same order as the difference between the approximate and exact solutions.

E. Ray approximation

A plane-wave or ray approximation can frequently provide helpful insight into the propagation characteristics of the multimode waveguide. In a step-index waveguide, a mode can be approximated by a plane wave or a congruence of rays (Maurer and Felsen, 1970) propagating at an angle θ defined as

$$\cos\theta = \beta/n_1 k . \tag{2.54}$$

Using the WKB expression for β gives

$$\theta = \sqrt{2\Delta}\ (m/M) \tag{2.55}$$

for the step-index profile.

For the graded-index fiber the plane-wave concept does not apply, but it is still illuminating to consider a mode as a congruence of rays whose propagation angle $\theta(r)$ varies with position. Defining $\theta(r)$ as

$$\cos\theta(r) = \beta/n(r)k \tag{2.56}$$

and using the WKB result, Eq. (2.50), for α-class profiles give the relation (Olshansky *et al.*, 1977)

$$m/M = [(r/a)^\alpha + \theta^2/2\Delta]^{(\alpha+2)/2\alpha}. \tag{2.57}$$

Equation (2.57) is useful for estimating the model excitation pattern produced by a specified launch condition.

F. Pulse propagation

Modal delay times, calculated from the guided mode propagation constants, are required for analysis of pulse broadening in the multimode optical waveguide and for calculation of its information-carrying capacity. In practice, the information bandwidth of the waveguide is greatly affected by the dispersion of the glass medium (Olshansky and Keck, 1976) and by the source spectral linewidth (Gloge, 1971a; DiDomenico, 1972). The effects of dielectric dispersion are discussed in Sec. III. Here it is assumed that the medium is dispersionless, that is,

$$\frac{dn}{d\lambda} = 0 \quad \text{for all } \lambda. \tag{2.58}$$

Because of the k dependence of the phase factor, $\exp(i\beta_{\mu\nu}z)$, in the field solution Eq. (2.5), a pulse of radiation will propagate with a delay time

$$\tau_{\mu\nu} = \frac{z}{c}\frac{d\beta_{\mu\nu}}{dk}, \tag{2.59}$$

where c is the speed of light. After expanding the expression Eq. (2.50) for the modal propagation constant of α-class profiles in powers of Δ, one finds the result (Gloge and Marcatili, 1973)

$$\tau_{\mu\nu} = \frac{zn_1}{c}\left[1 + \Delta\left(\frac{\alpha-2}{\alpha+2}\right)\left(\frac{m}{M}\right)^{2\alpha/\alpha+2} + \frac{\Delta^2}{2}\left(\frac{3\alpha-2}{\alpha+2}\right)\left(\frac{m}{M}\right)^{4\alpha/\alpha+2} + O(\Delta^3)\right]. \tag{2.60}$$

For $\alpha = 2$, the modal delay differences vanish to first order in Δ. If one chooses $\alpha = 2 - 2\Delta$, the $m = 1$ and $m = M$ modes have the same delay time, and an extra reduction in pulse broadening is achieved (Gloge and Marcatili, 1973).

The rms impulse response for uniform excitation, defined as

$$\sigma = \left\{\int_0^M \frac{2mdm}{M^2}\tau^2(m) - \left[\int_0^M \frac{2mdm}{M^2}\tau(m)\right]^2\right\}^{1/2}, \tag{2.61}$$

is a useful measure of the pulse broadening (Personick, 1973). For α-class profiles, the rms pulse width is minimized if (Olshansky and Keck, 1976)

$$\alpha = 2 - 12\Delta/5 \tag{2.62}$$

and the minimum pulse broadening is given as

$$\sigma_{\min} = \frac{z}{c}\frac{n_1}{\sqrt{12}}\Delta^2/10. \tag{2.63}$$

For a step-index waveguide, the corresponding pulse width is

$$\sigma_{\text{step}} = \frac{z}{c}\frac{n_1}{\sqrt{12}}\Delta. \tag{2.64}$$

Thus the optimal α profile reduces pulse broadening by $\Delta/10$, or about three orders of magnitude for a typical multimode waveguide.

An approximate measure of the information bandwidth B_w can be obtained from the expression (Personick, 1973)

$$B_w = 0.2/\sigma, \tag{2.65}$$

where B_w is given in gigahertz and σ in nanoseconds. Equation (2.65) gives the 3 dB bandwidth of a Guassian pulse with rms width σ and is a good approximation for other pulse shapes. For the step-index waveguide with $\Delta = 0.01$, the rms pulse broadening is 14 ns/km corresponding to an estimated bandwidth of 14 mHz-km. For the optimal α profile, the broadening is 0.014 ns/km and the estimated bandwidth is 14 gHz-km.

Several studies (Cook, 1977; Ishikawa *et al.*, 1977) have shown that the introduction of an additional term to the α-class profile provides a new degree of design flexibility which can be exploited to further reduce the pulse broadening below the rate obtained for the best α profile. Although this concept is indeed correct, it is not clear that the approximation used in these calculations has sufficient accuracy to determine the optimal values of the profile parameters.

G. Effect of the cladding

In the Laguerre–Gauss solution for the parabolic profile, and in the WKB approximation, the cladding is ignored. The graded-index profile is treated as though it extended to infinity and a mode cutoff is artificially imposed at β equal to n_2k.

The presence of a uniform refractive index cladding leads to a substantial correction for the fields of a parabolic slab waveguide (Hashimoto, 1976). Studies based on variational techniques have shown that the delay times (Okamoto and Okoshi, 1976) of the highest-order guided modes of the fiber are significantly altered. The effect of the cladding can also be treated in the WKB approximation (Olshansky, 1977a). In a typical parabolic waveguide the majority of the modes are unaffected by the cladding, but the delay times of 5% of the highest-order modes are decreased by as much as several ns/km.

If the highest-order modes are unattenuated, Okamoto and Okoshi (1977a) have shown that the delay time shift can be corrected by introducing an index valley between the core and uniform index cladding. However, only 0.2 dB of high-order mode loss is required to attenuate the affected modes (Olshansky, 1977a). In any practical communication system, bending losses, splice losses, or other geometrical perturbations are likely to attenuate the highest-order guided modes and make the index valley unnecessary.

H. Leaky modes

In addition to the guided modes, having propagation constants in the range $n_1k > \beta > n_2k$, there exists a class of modes, called leaky modes, which are only partially confined within the core of the waveguide (Snyder and Mitchell, 1974; Snyder *et al.*, 1974). The existence of leaky modes can be understood from the effective index profile shown in Fig. 3. The presence of the angular momentum term introduces an angular momentum barrier shown by the shaded area. Modes having the real part of β in the range

$$n_2k > \mathrm{Re}\,\beta > \sqrt{(n_2k)^2 - \nu^2/a^2} \tag{2.66}$$

are partially bound within the core, but can tunnel through the angular momentum barrier and radiate into the cladding. These modes are equivalent to the well-known resonant states of quantum mechanics. Snyder and coworkers (Snyder and Mitchell, 1974; Snyder, Mitchell, and Pask, 1974; Snyder, White, and Mitchell, 1975) were the first to predict the existence of leaky modes and to derive their attenuation rates in step-index fibers. For graded-index fibers the mode volume of leaky modes has been analyzed (Adams *et al.*, 1975; Stewart, 1975b) and their attenuation coefficients calculated (Petermann, 1975; Olshansky, 1976b; Snyder and Love, 1976b).

In the WKB approximation the leaky mode attenuation rates for a parabolic profile are of the form

$$\gamma_{\mu\nu} = \frac{1}{\pi}\,\frac{(2\Delta)^{1/2}}{a}\exp(-2\phi_2)\,, \tag{2.67}$$

where ϕ_2 is a WKB-type integral across the angular momentum barrier. The exact expression is given in the Appendix. Most leaky modes attenuate very rapidly, at rates as great as 10^4 dB/m. However, a few leaky modes, particularly those with large ν and β nearly equal to n_2k, must tunnel through a very wide angular momentum barrier. Their attenuation rates can be less than 0.1 dB/km and, practically speaking, they are indistinguishable from guided modes. Leaky mode attenuation coefficients for a typical parabolic profile waveguide are shown in Fig. 4. For fixed m (constant β), the loss decreases as ν increases because of the increasing size of the angular momentum barrier. For fixed ν, loss increases as m increases because the effective barrier becomes smaller.

Love and Pask (1976) have calculated universal curves for the decay rate of total leaky mode power in step and parabolic profiles. In a typical multimode waveguide, if all guided and leaky modes are initially excited, after 1 m of propagation 10%–30% of the remaining power is predicted to reside in leaky modes. After 1 km this fraction is reduced to 10%–20%. Thus, for the ideal waveguide, leaky modes are predicted to have a large influence on measurements of a waveguide's optical properties, particularly on a measurement, such as the near-field profile (Sladen *et al.*, 1975; Arnaud and Derosier, 1976), which is made on a short (~1 m) length of fiber.

Although leaky modes have been observed (Stewart, 1975a; Zemon and Fellows, 1976), they appear to attenuate much more rapidly than predicted. Near-field

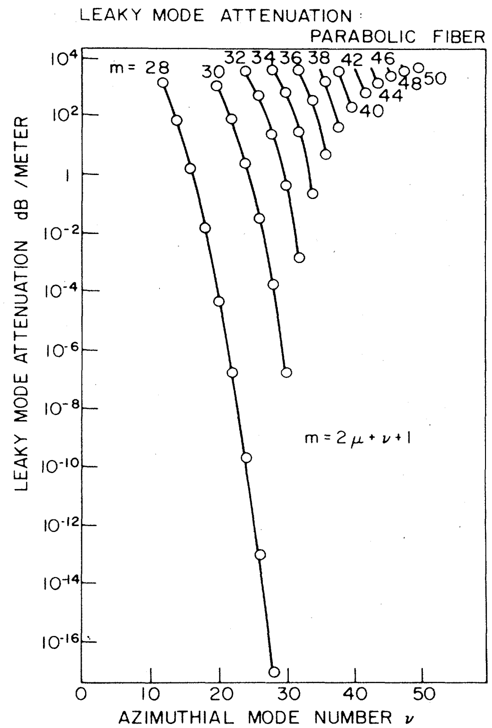

FIG. 4. Leaky mode attenuation rates predicted for a typical parabolic profile waveguide.

profiles uncorrected for leaky modes agree better with the actual index profile (Arnaud and Derosier, 1976; Costa and Sordo, 1976) and lead to better predictions of pulse broadening (Olshansky and Keck, 1976). Leaky mode propagation over kilometer lengths of waveguide has not been reported.

Petermann (1977a, 1977b) has shown that a small ellipticity causes a large increase in leaky mode attenuation rates, particularly in parabolic index profiles. Leaky mode losses also increase in the presence of index profile perturbations randomly varying along the fiber length (Olshansky and Nolan, 1977).

III. EFFECT OF THE GLASS MEDIUM ON WAVEGUIDE PROPAGATION

In the previous section, the waveguide medium was treated as an ideal, lossless, dispersionless dielectric. In practice, the optical properties of the glass play a critical role in determining the attenuation rates and information bandwidths that can be achieved. These important properties of optical waveguide glasses are discussed in this section.

Although much of the discussion presented here is applicable to any glass composition, many specific references will be made to doped deposited silica glasses (Maurer and Schultz, 1972) containing GeO_2 (Keck, Maurer, and Schultz, 1973; MacChesney *et al.*, 1974; Maurer and Schultz, 1975), B_2O_3 (Kato, 1973; French *et al.*, 1973), and P_2O_5 (Payne and Gambling, 1974). These compositions are conveniently made by the vapor phase oxidation method (Keck and Schultz, 1973; Keck, Schultz, and Zimar, 1973; Schultz, 1973; MacChesney *et al.*, 1974) and presently considered to be the choice dopants for waveguides used in telecommunication systems.

A. Attenuation

In optical quality glasses prepared by conventional melting techniques, the primary source of attenuation is absorption from transition element impurities. The absorption losses in dB/km per part per billion weight (ppbw) of the more common metallic ions are listed in Table I (Schultz, 1974; Bates, 1962), along with the wavelength of the absorption peak. The absorption of the elements varies critically with oxidation state. For telecommunication applications, transition element contamination must either be kept below a few ppbw or the oxidation state must be controlled.

The vapor phase oxidation technique has provided a simple and practical method for achieving these purity levels. High-purity raw materials such as $SiCl_4$, $GeCl_4$, BCl_3, and $POCl_3$ are readily available and can be oxidized under controlled conditions to form the corresponding oxide glasses. Recent results (Osanai *et al.*, 1976) indicate that the effect of metallic impurities can be reduced below 0.1 dB/km in the wavelength range of interest for telecommunications.

Progress in the double crucible melting technique (for a review see Newns, 1977) has shown that by starting with high-purity oxides, optical waveguides can be made with impurity absorption of only a few dB/km.

Once the effects of metallic impurities are eliminated, the remaining material losses are caused by intrinsic properties of the glass, O–H absorption bands, and drawing-induced absorption bands. In the spectral range between 0.6 and 1.3 μm, there is a broad window where intrinsic absorption is small or negligible. At the shorter wavelengths, there is an ultraviolet absorption tail or Urbach edge (Urbach, 1953) which decreases exponentially from the electronic band edge. At longer wavelengths, there is an exponential tail from the infrared vibrational bands (Osanai *et al.*, 1976; Izawa *et al.*, 1977; Bagley *et al.*, 1976).

Within this broad window, the dominant intrinsic losses are Rayleigh scattering losses from density and concentration fluctuations frozen into the glass lattice (Keck, Maurer, and Schultz, 1973; Pinnow *et al.*, 1973). In the critical range from 0.8–0.9 μm where GaAs and GaAlAs solid state sources operate, Rayleigh scattering is the only important intrinsic loss source.

TABLE I. Absorption rates in dB km^{-1} ppbw^{-1} of some of the more common metallic ions and the wavelength of the absorption peak.

	λ_{peak} (nm)	dB km^{-1} ppbw^{-1} (800 nm)
Cr^{3+}	625	1.6
Co^{2+}	685	0.1
Cu^{1+}	<300	<0.01
Cu^{2+}	850	1.1
Fe^{2+}	1100	0.68
Fe^{3+}	<400	0.15
Ni^{2+}	650	0.1
Mn^{3+}	460	0.2
V^{4+}	725	2.7

1. Ultraviolet absorption edge

The UV edge of the electronic absorption bands of amorphous and crystalline materials are well described by the empirical relationship (Urbach, 1953)

$$\gamma_{UV} = C\exp(E/E_0) \tag{3.1}$$

known as Urbach's rule, where E is the photon energy and C and E_0 are empirical constants. At lower energies, secondary exponential edges are commonly observed (for a discussion see Tauc, 1976). In several instances, the secondary edge has been identified as a charge transfer impurity absorption band, but in other cases the secondary edge may be related to structural defects of the material. Since the ultraviolet absorption edge of optical waveguide glasses can in principle extend into the near infrared, its origin and magnitude are of interest.

For fused silica, the reported values for the primary Urbach edge (see Bates, 1977) extrapolate below 0.1 dB/km for wavelengths greater than 0.23 μm. Whether there are "intrinsic" secondary ultraviolet edges which extend to longer wavelengths is unknown. There appears to be no evidence of intrinsic SiO_2 absorption contributing measurably to waveguide attenuation in the near infrared. In view of the comparable ultraviolet transparency of B_2O_3, the Urbach edge of borosilicas is also believed to be negligible in the near infrared.

For GeO_2 and P_2O_5 doped silicas, the bandgap is smaller and the Urbach edge is expected to shift to longer wavelengths. Measurements of ultraviolet absorption in GeO_2–SiO_2 fiber (Keck, Maurer, and Schultz, 1973) and in bulk samples (Schultz, 1977) show the presence of a GeO_2 band at 0.24 μm whose Urbach edge is negligible for $\lambda \geq 0.4$ μm. A secondary edge (Keck, Maurer, and Schultz, 1973; Osanai *et al.*, 1976) contributing about 0.2 dB/km at 0.82 μm and 10 dB/km at 0.5 μm has also been observed. Measurements of more recent fibers (Olshansky, 1977b) have failed to show this secondary edge.

2. Infrared absorption edge

At longer wavelengths, there exist absorption bands produced by the silicon–oxygen, and cation–oxygen vibrational modes. The location and identification of these bands are given in some recent references: for SiO_2, Spitzer *et al.*, 1961; for GeO_2, Izawa *et al.*, 1977; for B_2O_3, Tenney *et al.*, 1972 and Izawa *et al.*, 1977; and for P_2O_5, Wong, 1976. The fundamental vibrational band lies at the highest frequency and has an exponential tail extending into the region 1.3–1.6 μm at a significant absorption level. This IR edge has the exponential form

$$\gamma_{IR} = C_{IR}\exp(-E/E_0). \tag{3.2}$$

The frequency ω_f of the fundamental absorption peak satisfies the approximate relation

$$\omega_f \propto (\mu_R)^{-1/2}, \tag{3.3}$$

where μ_R is the reduced mass of the cation–oxygen pair. Thus for a dopant cation such as Ge which is heavier than Si, ω_f is smaller and the infrared absorption in the region below 2 μm is reduced. However, for boron, with atomic mass of 10.8, the boron–oxygen vi-

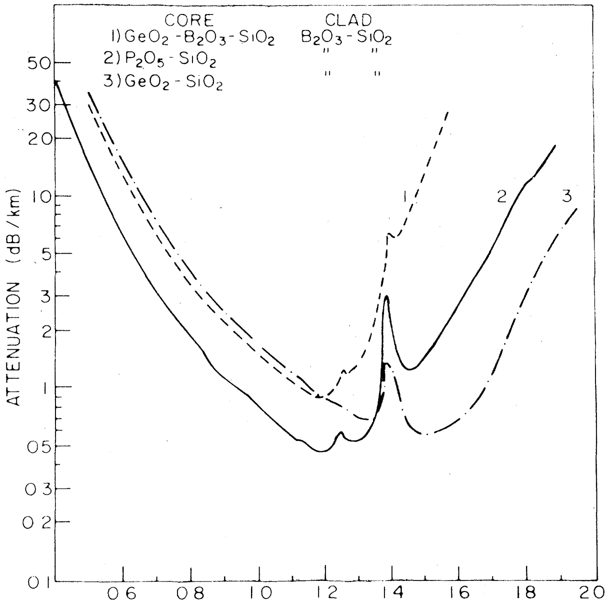

FIG. 5. Spectral attenuation rates measured for three very-low-loss optical waveguides (after Osanai *et al.*, 1976).

brational band is shifted to higher frequencies and boron-doped waveguides show significantly increased infrared absorption. These trends can be seen in the spectral attenuation data obtained (Osanai *et al.*, 1976) on 1-km fibers and shown in Fig. 5. If optical waveguides are operated at wavelengths greater than 1.2 μm, lowest losses will be obtained in B_2O_3-free compositions.

3. Rayleigh scattering

In the low absorption window lying between the ultraviolet and infrared absorption tails, the dominant intrinsic source of waveguide attenuation is scattering losses from refractive index fluctuations frozen into the glass lattice. These losses follow the characteristic λ^{-4} Rayleigh scattering law. In the important spectral region 0.8–1.1 μm they are the only significant intrinsic loss mechanism.

The lowest value reported for Rayleigh scattering in bulk SiO_2 is 3.9 dB/km at 0.6328 μm (Schroeder *et al.*, 1973). Rayleigh scattering does vary with sample quality, and the values 4.8 dB/km (Maurer, 1973) and 5.4 dB/km (Rich and Pinnow, 1972) have also been reported for bulk SiO_2. At 0.8 μm the lowest attainable loss for SiO_2 is thus predicted to be 1.5 dB/km.

In multicomponent glasses, the Rayleigh scattering can be greater or less than that of fused silica, and the dependence of these losses on composition is of considerable interest. The physics of Rayleigh scattering in glasses is a complex subject (see Fabelinskii, 1967) and the scattering levels observed in optical waveguides are not well understood on the basis of first principles. In the following paragraphs, some of the theoretical and experimental work on this subject is reviewed.

Scattering from refractive index fluctuations frozen into the glass lattice is given as

$$\gamma_{\rm RS}=\frac{8\pi^3}{3\lambda^4}\,\overline{(\delta n^2)^2}\,\delta V\,, \tag{3.4}$$

where $\overline{(\delta n^2)^2}$ is the mean-squared fluctuation in refractive index-squared and δV is the volume over which it occurs.

For multicomponent glasses

$$\overline{(\delta n^2)^2}=\left(\frac{\partial n^2}{\partial\rho}\right)^2\overline{(\delta\rho)^2}+\sum_i\left(\frac{\partial n^2}{\partial C_i}\right)^2\overline{(\delta C_i)^2}\,, \tag{3.5}$$

where $\delta\rho$ is the density fluctuation and δC_i is the concentration fluctuation of the ith glass component.

Statistical mechanics (see Landau and Lifshitz, 1958) gives

$$\frac{\overline{(\delta\rho)^2}}{\rho^2}=\frac{\beta_c}{\delta V}\,K_BT_F\,, \tag{3.6}$$

where β_c is the isothermal compressibility evaluated at the fictive temperature T_F, and K_B is Boltzmann's constant. The concentration fluctuations are given as

$$\overline{(\delta C_i)^2}=\frac{K_BT_F}{N_i\partial\mu_c/\partial C_i}\,, \tag{3.7}$$

where N_i is the number of moles per unit volume of component i and μ_c is the chemical potential.

In a single-component glass only density fluctuations can occur. From the definition of the photoelastic coefficient p, one can derive the relation (Schroeder *et al.*, 1973; Pinnow *et al.*, 1973)

$$\left(\rho\frac{\partial n^2}{\partial\rho}\right)=n^4p \tag{3.8}$$

and thus

$$\gamma_{\rm RS}=\frac{8\pi^3}{3\lambda^4}\,n^8p^2\beta_cK_BT_F\,. \tag{3.9}$$

Alternatively, from the Lorentz–Lorenz formula one finds the approximate relation

$$n^2\approx 1+\rho\delta n^2 \tag{3.10}$$

and

$$\left(\rho\frac{\partial n^2}{\partial\rho}\right)^2=(n^2-1)^2\,. \tag{3.11}$$

Equations (3.4)–(3.6) and (3.11) thus give (Stacey, 1956; Maurer, 1973)

$$\gamma_{\rm RS}=\frac{8\pi^3}{3\lambda^4}\,(n^2-1)^2\beta_cK_BT_F\,. \tag{3.12}$$

For an annealed sample of fused silica, the fictive temperature is estimated as 1400 °K, the high-temperature isothermal compressibility is 6.8×10^{-12} cm^2/dyn (Laberge *et al.*, 1973), and the photoelastic coefficient is 0.286 (Schroeder *et al.*, 1973). At 0.6328 μm, Eq. (3.9) gives 4.9 dB/km and Eq. (3.12) gives 3.7 dB/km, in reasonable agreement with the reported values for scattering in fused SiO_2. Both Eq. (3.9) and Eq. (3.12) indicate that lower scattering from density fluctuations is expected in low-temperature, low-index, low-compressibility glasses. In fact, scattering losses as low as 25% of the value for fused silica have been reported for alkali–aluminosilica glasses (Gupta *et al.*, 1975; Pinnow *et al.*, 1975), which have both low index ($n\approx1.5$) and low fictive temperature (~700 °K).

Estimates of Rayleigh scattering in multicomponent glasses must include the additional effect of concentration fluctuations. If phase separation or clustering does not occur, the assumption of ideal mixing provides a plausible model. As an illustration, consider a system consisting of SiO_2 plus a single dopant. The Rayleigh scattering γ_c due to the difference in molecular polarizability can be written as

$$\gamma_c = \frac{8\pi^3}{3\lambda^4}\left(\frac{\partial n^2}{\partial N}\right)(\delta N)^2 , \tag{3.13}$$

where N is the number of dopant molecules per unit volume and $(\delta N)^2$ is the mean-squared fluctuation of N due to ideal mixing. Elementary statistics give

$$(\delta N)^2 = C(1-C)\frac{\rho N}{M} , \tag{3.14}$$

where C is the mole concentration of the dopant, M its gram-molecular weight, and ρ its density.

This model can be illustrated by considering the GeO_2–SiO_2 binary system. The index-squared is well described by a linear form (Fleming, 1976; Kobayashi *et al.*, 1977)

$$n^2 = n_S^2 + C(n_G^2 - n_S^2) , \tag{3.15}$$

where n_S and n_G are, respectively, the refractive indices of fused SiO_2 and fused GeO_2. With the values $n_S = 1.458$, $n_G = 1.603$, $\rho_G = 3.6$ g/cm^3, and $M_G = 104.6$, one finds the concentration fluctuations are given as

$$\gamma_c = \frac{C(1-C)}{\lambda^4} 3.3\ \mathrm{dB/km^{-1}}\ \mu\mathrm{m}^{-4} . \tag{3.16}$$

At low GeO_2 concentrations, this is about 0.07 dB km^{-1} mol %$^{-1}$ GeO_2 at 0.82 μm. It is not possible to directly compare this number with measured values because the effect of GeO_2 on density fluctuations is not known. The number derived from Eq. (3.16), however, is not too different from the total increase in scattering of 0.05 dB km^{-1} mol%$^{-1}$ GeO_2 observed in optical waveguides (Yoshida *et al.*, 1977).

Measurements of bulk samples show that ideal mixing fails badly for Na_2O–SiO_2 glasses. Gupta *et al.* (1975) conclude that alkali–silica and alkali-aluminosilica glasses are nonequilibrium, nonideal solutions.

A number of workers have reported empirical relationships between Rayleigh scattering and optical waveguide composition. O'Connor *et al.* (1976) find the scattering increases linearly with numerical aperture (NA) in GeO_2-SiO_2 waveguides containing a small amount of B_2O_3. Gambling, Payne, Hammond and Norman (1976) report that in P_2O_5-SiO_2 waveguides, the scattering increases linearly with P_2O_5 concentrations. Sommer *et al.* (1976) have reported a 1 dB/km decrease in scattering at 0.82 μm upon substituting a small amount of P_2O_5 for B_2O_3 in a GeO_2–SiO_2 waveguide. A more detailed study of this effect (Yoshida *et al.*, 1977) has found that, for comparable values of Δ, substitution of P_2O_5 for B_2O_3 reduces scattering losses by 25–30%. The data are summarized in Fig. 6, where Rayleigh scattering in dB/km at 1 μm is plotted versus Δ in percent.

The lowest Rayleigh scattering value, 0.6 dB/km at 1 μm, has been reported (Horiguchi and Osanai, 1976) for a 0.18 NA P_2O_5–SiO_2 waveguide containing 2 mole% P_2O_5 in the core and 14 mole% B_2O_3 in the cladding (Horiguchi, 1978).

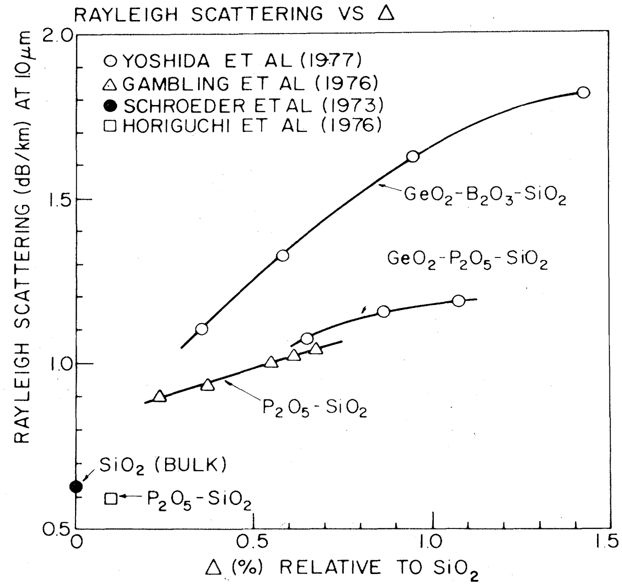

FIG. 6. Rayleigh scattering at 1.0 μm is plotted vs Δ for different compositions. All data except for fused SiO_2 are from fiber samples.

In addition to the intrinsic loss sources, there are two kinds of nonintrinsic losses which play an important role in optical waveguides. The first is absorption from the harmonics and sidebands of the fundamental O–H vibrational band at 2.8 μm. The second is absorption from various drawing-induced defects or color centers which have been observed.

4. O-H absorption bands

Early work (Keck, Maurer, and Schultz, 1973; Kaiser *et al.*, 1973) reported on the presence of various O–H bands in a low-loss optical waveguide. These results are reproduced in Fig. 7. If the O–H level is kept

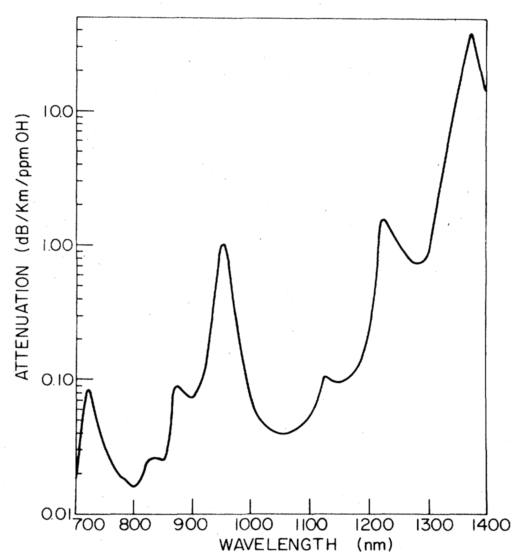

FIG. 7. The O–H absorption band observed in a GeO_2–SiO_2 optical waveguide (after Keck, Maurer and Schultz, 1973).

below a few parts per million (ppm), the only significant band in the region below 1.15 μm is the second overtone at 0.95 μm, which absorbs at a rate of about 1 dB km^{-1}ppm^{-1}. At longer wavelengths, the first overtone at 1.38 μm and its sideband at 1.25 μm are strong absorbers. At 1.25 μm, the O–H absorption is about 2 dB km^{-1}ppm^{-1}, and at 1.25 μm it is about 40 dB km^{-1}ppm^{-1}.

Using specially purified reactants, it has been possible (see Fig. 5) to reduce the O–H content to as low as 50 ppb (Horiguchi and Osanai, 1976; Osanai *et al.*, 1976). With this very low O–H content, total attenuation rates as low as 0.5 dB/km have been achieved at 1.2 μm.

The position of the fundamental O—H band is reported to be shifted to 3.1 μm in phosphosilica waveguides (Mita *et al.*, 1977).

5. Drawing-induced absorption bands

The rapid quenching which occurs during the drawing process can result in the presence of nonequilibrium oxidation states for any of the cations or ionic complexes present in the glass. These states can give rise to optical absorption bands which are referred to as drawing-induced coloration or defect bands.

The presence of a drawing-induced absorption band at 0.62 μm in fused-silica optical fibers was first reported by Kaiser (1974). He found that this band can be eliminated by heat treatment of the fiber after it is drawn. Although the band is occasionally present in GeO_2–SiO_2 fibers, it usually produces only a few dB/km excess loss at its peak and does not extend into the 0.8–0.9 μm range. Excess scattering associated with this band can increase the measured scattering at 0.6328 μm (Kaiser, 1974). If this is not taken into account, measured scattering may be misinterpreted as anomalously high Rayleigh scattering.

A more troublesome drawing-induced absorption band appears at 0.55 μm in P_2O_5–SiO_2 fibers. This band can be very large and broad, contributing excess losses as high as a few dB/km at 0.8 μm. Modifications of draw conditions (Yoshida *et al.*, 1977) or subsequent heat treatment (Yamauchi *et al.*, 1977) can be used to eliminate this source of attenuation.

This completes the discussion of the sources of loss introduced by the glass medium. Additional attenuation can result from deviations from the ideal geometry and index profile. Such effects are discussed in Sec. IV.

B. Pulse broadening

In Sec. II, the glass medium is treated as a dispersionless dielectric. In practice, refractive index dispersion significantly affects optical waveguide pulse propagation in two ways. As a consequence of index dispersion, modal delay times τ_m depend on wavelength. Pulse spreading occurs in proportion to both the derivative of τ_m and the source spectral width. Refractive index dispersion also influences the mode dependence of τ_m, and this affects the choice of index profile which minimizes intermodal pulse broadening.

1. Intramodal pulse broadening

The rms intramodal pulse broadening σ_s is approximately given as

$$\sigma_s = \frac{L}{c}\left|\lambda\frac{d^2n_1}{d\lambda^2}\right|\sigma_\lambda , \qquad (3.17)$$

where L is the waveguide length and σ_λ is the rms source spectral width. This type of pulse broadening is frequently referred to as material or chromatic dispersion.

GaAlAs LED's, emitting between 0.8 and 0.9 μm typically have spectral widths on the order of 20 nm. At 900 nm, $|\lambda^2 dn^2/d\lambda^2|$ is about 0.02 for GeO_2–SiO_2 glasses (Fleming, 1976; Kobayashi *et al.*, 1977) so that the spectrally induced broadening is on the order of 1.5 ns/km for LED sources. This is small compared to the 15 ns/km pulse broadening caused by modal delay differences in a step waveguide [see Eq. (2.64)], but it is an order of magnitude greater than the intermodal broadening which can now be routinely achieved by proper grading of the index profile.

For conventional GaAs and GaAlAs injection lasers, spectral widths are in the range of 1–2 nm. The resulting pulse broadening of 0.08–0.15 ns/km is greater than the intermodal broadening of the best graded-index fibers which have been reported (Keck and Boullie, 1978).

Recently, the successful fabrication of single-longitudinal-mode GaAs lasers has been reported (Ikeda *et al.*, 1977; Nakamura *et al.*, 1977). They have linewidths less than 0.1 Å. For systems operating with this type of source, intermodal delay differences will be the dominant factor limiting transmission bandwidth.

As a function of wavelength the refractive index of any glass has an inflection point, $d^2n/d\lambda^2 = 0$, in the infrared. Figure 8 shows a plot of $\lambda^2 d^2n/d\lambda^2$ vs λ for fused silica (Malitson, 1965) and GeO_2–SiO_2 glass containing 7.9 mol% GeO_2 (Kobayashi *et al.*, 1977).

At the inflection point the first-order calculation of spectral pulse broadening, Eq. (3.17), is zero (hence

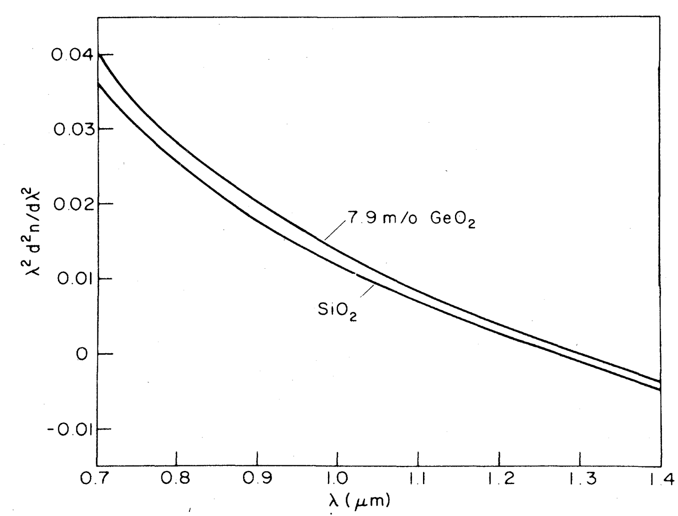

FIG. 8. $\lambda^2 dn^2/d\lambda^2$ vs λ for SiO_2 (Malitson, 1965) and 7.9 mol% GeO_2 (Kobayashi *et al.*, 1977).

the name "zero material dispersion" point) and the next higher-order term must be included (Kapron, 1977; Payne *et al.*, 1978). The resulting intramodal broadening, however, is still reduced by at least an order of magnitude.

Thus for multimode waveguides with minimized intermodal pulse broadening, very low pulse broadening can be achieved using either LED's or conventional injection lasers by operating at the zero material dispersion wavelength.

The wavelength of the inflection point varies with composition. Bulk sample index measurements show that for fused silica it occurs at 1.27 μm, while for GeO_2-doped silica it moves to larger wavelengths, and for B_2O_3-doped silicas to shorter wavelengths. This effect has been confirmed by direct measurements of modal delay shifts as a function of wavelength for GeO_2-doped fibers (Cohen and Lin, 1977; Payne and Hartog, 1977; Lin *et al.*, 1978) and B_2O_3-doped fibers (Cohen and Lin, 1977). The inflection point of P_2O_5-doped silica appears to be the same as for SiO_2 (Payne and Hartog, 1977; Lin *et al.*, 1978).

From the Kramers–Kronig dispersion relation for the dielectric constant it follows that the location of the inflection point depends on cancellation between contributions from the electronic and the vibration absorption bands. The contribution of the electronics bands of B_2O_3 are similar to SiO_2 while the B–O vibrational bands are at shorter wavelengths and give a larger contribution than the Si–O vibrational bands. Thus, as the B_2O_3 dopant level increases, the inflection point moves to shorter wavelengths. For GeO_2-doped silicas both electronic and vibrational bands shift to longer wavelengths and so does the inflection point.

2. Intermodal pulse broadening

The total rms pulse broadening is given as

$$\sigma=(\sigma_s^2+\sigma_m^2)^{1/2}, \tag{3.18}$$

where σ_s is the intramodal or spectral broadening, just discussed, and σ_m is the broadening caused by delay differences among the modes. While σ_s is proportional to the second derivative of the core glass refractive index, σ_m depends on the difference between the first derivatives of the refractive index at $r=0$ and $r=a$.

a. α profiles

From the expression for $\beta_{\mu\nu}$ given by Eq. (2.50) for α-class index profiles and from Eq. (2.59) one finds that the modal delay times are (Olshansky and Keck, 1976)

$$\tau_{\mu\nu}=\frac{LN_1}{c}\left[1+\left(\frac{\alpha-2+2P}{\alpha+2}\right)\Delta\left(\frac{m}{M}\right)^{(2\alpha)/(\alpha+2)} +\left(\frac{3\alpha-2}{\alpha+2}\right)\frac{\Delta^2}{2}\left(\frac{m}{M}\right)^{(4\alpha)/(\alpha+2)}\right]+O(\Delta^3), \tag{3.19}$$

where

$$N_1=n_1-\lambda dn_1/d\lambda \tag{3.20}$$

and

$$P=\frac{n_1}{N_1}\frac{\lambda}{\Delta}\frac{d\Delta}{d\lambda}. \tag{3.21}$$

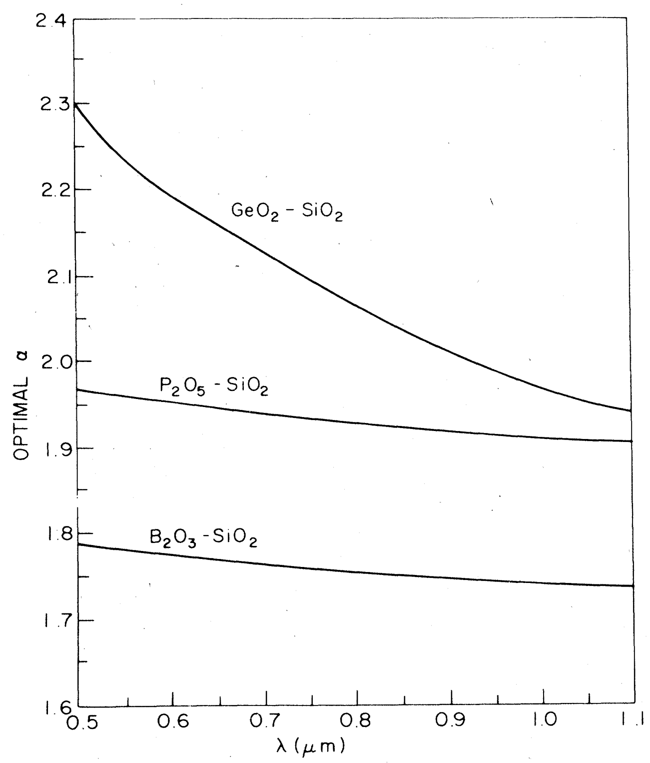

FIG. 9. The dependence of the optimal α profile with wavelength for different waveguide compositions (after Presby and Kaminow, 1976).

Minimal rms pulse broadening is realized if the fiber has an optimized profile given by

$$\alpha_0=2-2P-\tfrac{12}{5}\Delta. \tag{3.22}$$

The correction term P varies considerably with λ and composition (Presby and Kaminow, 1976; Fleming, 1976). The optimal α for several compositions is shown in Fig. 9.

Experimental verification of Eq. (3.22) has been reported by Cohen (1976). Using B_2O_3–SiO_2 waveguides with different α profiles, he measured pulse broadening by the shuttle pulse technique (Cohen, 1975). The observed pulse broadening agrees well with the prediction of an optimal α of 1.8 for the B_2O_3–SiO_2 composition.

In evaluating expressions such as Eq. (3.22) it is important to be aware that the refractive index and its derivatives can vary significantly according to the sample's thermal history. This is particularly true for B_2O_3-doped glasses, which are known to show a large quenching effect (Wemple *et al.*, 1973). As shown in Table II, the index change in a fiber per mol% B_2O_3 ranges from -0.52×10^{-3} to -1.00×10^{-3} (Presby and Kaminow, 1976; French *et al.*, 1976; Hammond and Norman, 1977). The index change deviates from a linear dependence on composition at molar concentrations above 5%. The extent of the deviation appears to increase with the degree of quenching.

High-accuracy index data for preform samples of GeO_2–SiO_2 glasses show an index change of 1.57×10^{-3}/mol% GeO_2 (Fleming, 1976; Kobayashi *et al.*, 1977).

TABLE II. The index change Δn per mol% dopant (relative to silica), tabulated as it has been reported by different researchers.

Dopant	Sample	Δn/mol% $\times 10^{-3}$	Reference
GeO_2	Preform	1.57	Fleming, 1976; Kobayashi *et al.*, 1977
	Fiber	1.31	Hammond and Norman, 1977
B_2O_3	Preform	−0.10	Fleming, 1976
	Fiber	−0.56	French *et al.*, 1976
	Fiber	−0.52	Hammond and Norman, 1977
	Fiber	−(0.59−1.00)	Presby and Kaminow, 1976
P_2O_5	Preform	0.95	Katsuyama *et al.*, 1977
	Fiber	0.79	Katsuyama *et al.*, 1977
	Fiber	0.60	Hammond and Norman, 1977
	Fiber	0.84	Presby and Kaminow, 1976

Measurement of GeO_2–SiO_2 fibers (Hammond and Norman, 1977) using the near-field technique (Sladen *et al.*, 1975) gives the index change as 1.31×10^{-3}/mol% GeO_2. It is not clear whether the differences in these values is due to quenching effects or to differences in the GeO_2 determination.

A small quenching effect has been reported for P_2O_5–SiO_2 fibers (Katsuyama *et al.*, 1977). Because of an apparent difficulty in determining the P_2O_5 content of fiber samples, reported values for the index change per mol% P_2O_5 vary from 0.60×10^{-3} to 0.84×10^{-3} (Hammond and Norman, 1977; Katsuyama *et al.*, 1977; Presby and Kaminow, 1976).

These index data are summarized in Table II.

As a result of quenching effects, it is desirable to base calculations of the optimal α profile on index measurements of fiber samples. For GeO_2–SiO_2 glasses the most accurate index data available are for preform samples (Fleming, 1976; Kobayashi *et al.*, 1977). For B_2O_3–SiO_2 and P_2O_5–SiO_2 compositions, dispersion data for several fiber compositions are available (Presby and Kaminow, 1976). More recently dispersion data extending over the range 0.4–2.0 μm have been obtained for GeO_2–SiO_2, P_2O_5–SiO_2, and B_2O_3–SiO_2 samples by measuring numerical aperture as a function of wavelength (Sladen *et al.*, 1978). At present the data of Sladen *et al.* (1978) appear to yield the best determination of the optimal α value, particularly at the longer wavelengths.

To illustrate the variation in pulse broadening as a function of wavelength, data for a 7.9 mol% GeO_2 on-axis composition (Kobayashi *et al.*, 1977) and a fused silica cladding composition (Malitson, 1965) have been used to calculate $\alpha_0(\lambda)$ from Eq. (3.22). The result is shown in Fig. 10. From Eq. (3.19) the rms pulse broadening as a function of λ can be calculated. For a fiber profile optimized for minimal broadening at 0.85 μm, $\alpha=2.08$ and the spectral variation in broadening is shown in Fig. 11. Because of the variation of the optimal α value with wavelength, the minimum dispersion is observed for only a narrow spectral band. Although intermodal pulse broadening less than 0.04 ns/km is achieved over the important spectral region 0.8–0.9 μm, at longer wavelengths, $\lambda \geq 1.06$ μm, the intermodal pulse broadening is greater than 0.1 ns/km.

For some applications, it may be desirable to achieve minimum dispersion over a broader spectral range or at several different wavelengths. This not only allows for the possibility of wavelength multiplexing but also offers the user flexibility to change source wavelength as improved sources become available or as system requirements change.

Kaminow and Presby (1977) have shown that it is possible to find compositions such that

$$\frac{d\alpha_0}{d\lambda}=0 \tag{3.23}$$

at a specified wavelength. They have studied the P_2O_5–GeO_2–SiO_2 system and found that if the on-axis composition is silica doped with C mole% P_2O_5 and the composition at $r=a$ is silica doped with $0.086C$ mol% GeO_2, the optimal α is approximately flat over the range 0.6–1.1 μm.

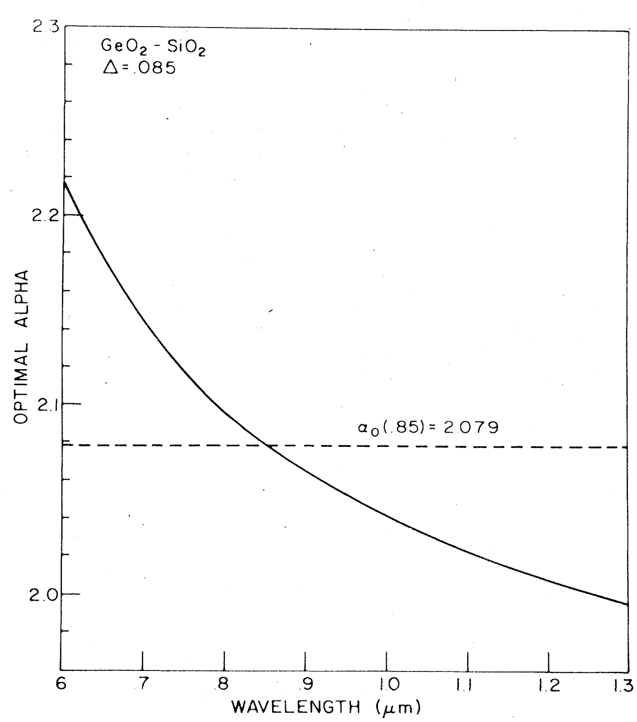

FIG. 10. The optimal α vs λ for a GeO_2–SiO_2 composition.

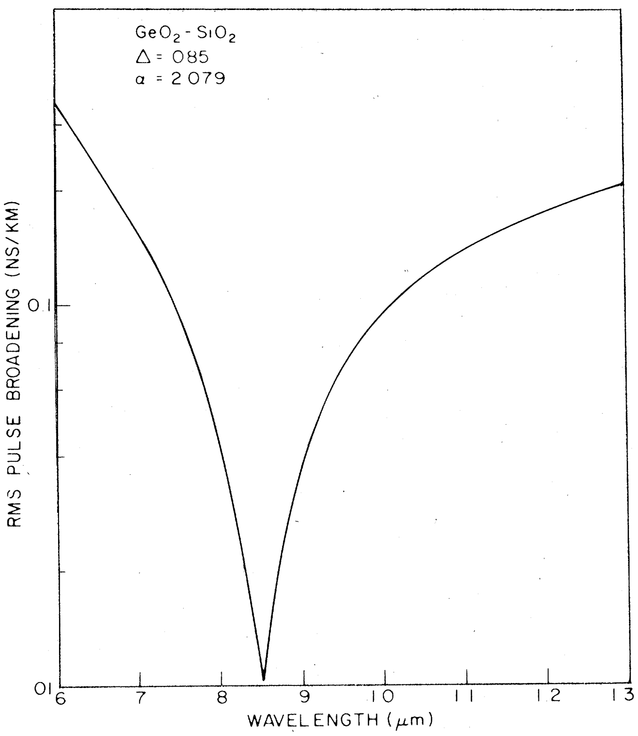

FIG. 11. Pulse broadening vs λ for a GeO_2–SiO_2 α profile designed for minimum dispersion at 0.85 μm.

b. Multiple-α profiles

Using the WKB method, Marcatili (1977) has shown that the modal delay time is of the form

$$\tau_{\mu\nu}=\frac{N_1 L}{c}\frac{1-B/D}{(1-B)^{1/2}}, \tag{3.24}$$

where

$$\beta_{\mu\nu}=n_1 k(1-B)^{1/2}. \tag{3.25}$$

Equation (3.24) is valid if the profile, defined as

$$n^2(r)=n_1^2[1-F(r,\lambda)], \tag{3.26}$$

satisfies the condition

$$\frac{1+(r/2F)(\partial F/\partial r)}{1-(n_1/2N_1)(\lambda/F)(\partial F/\partial\lambda)}=D(\lambda), \tag{3.27}$$

where D is a function of λ, not of r. This is a generalization of the result for α-class profiles. Equation (3.27) can be rewritten as a partial differential equation

$$r\frac{\partial F}{\partial r}+D\frac{n_1}{N_1}\lambda\frac{\partial F}{\partial\lambda}+2(1-D)F=0. \tag{3.28}$$

The α class of profiles, defined as

$$F(r,\lambda)=2\Delta(\lambda)(r/a)^{\alpha}, \tag{3.29}$$

satisfies Eq. (3.28) if

$$\alpha=2(D-1)-\frac{Dn_1}{N_1}\frac{\lambda}{\Delta}\frac{d\Delta}{d\lambda}. \tag{3.30}$$

The rms pulse dispersion is minimized for

$$D=2-6\Delta/5. \tag{3.31}$$

From the partial differential equation (3.28), it is clear that there are additional multiple-α solutions of the form (Olshansky, 1978)

$$F(r,\lambda)=\sum_{i=1}^{q}2\Delta_i(\lambda)(r/a)^{\alpha_i}, \tag{3.32}$$

where

$$\alpha_i=2(D-1)-\frac{Dn_1}{N_1}\frac{\lambda}{\Delta_i}\frac{d\Delta_i}{d\lambda},\quad i=1\cdots q. \tag{3.33}$$

The multiple-α profiles of Eqs. (3.32) and (3.33) have the same low dispersion as single-α profiles, but provide extra degrees of freedom for profile design. One has the freedom to specify how each of the d dopants is to be divided among the q terms of the profile. Assuming that the compositions at $r=0$ and $r=a$ are already specified, there are $d(q-1)$ new degrees of freedom which can be used to impose conditions on the $q\alpha_i(\lambda)$'s.

For example, with $q=2$ one could achieve low dispersion over an extended spectral range by requiring either

$$\frac{d\alpha_i}{d\lambda}=0 \text{ at } \lambda_0,\quad i=1,2, \tag{3.34}$$

or

$$\alpha_i(\lambda_1)=\alpha_i(\lambda_2),\quad i=1,2. \tag{3.35}$$

A condition such as Eq. (3.34) or Eq. (3.35) imposed on a single-α profile ($q=1$) specifies a particular composition which is not necessarily compatible with all the other fabrication constraints. The multiple-α profiles introduce a further degree of complexity to waveguide fabrication, but have the advantage of extending the range of compositions for which conditions such as Eq. (3.34) or Eq. (3.35) can be satisfied.

c. α profile plus correction terms

To achieve even lower intermodal dispersion, several authors have considered the addition of an $(r/a)^4$ term (Cook, 1977; Ishikawa *et al.*, 1977) or an $(r/a)^{2\alpha}$ term (Geckeler, 1977) to the α-class of profiles. Optimization of this class of profiles reduces the minimum rms pulse width by more than an order of magnitude. While it is clear from these studies that addition of small correction terms to the profile can reduce the intermodal broadening below that obtainable for a pure α-class profile, it is not clear that the approximation methods used in calculating modal delay times have sufficient accuracy to determine small corrections to the optimal profile shape. Further work is required to understand the uncertainties introduced by the use of the scalar wave equation [Eq. (2.16)] and by the WKB method of solution.

d. Compensation for nonlinear dispersion

The theory of the optimal α profile is based on the assumption that the profile shape [Eq. (2.44)] is maintained over the spectral width of the source. This is true if $dn^2/d\lambda$ is proportional to n^2 over the range of n^2 in the core of the fiber. Arnaud and Fleming (1976) have reported a calculation based on bulk index measurements of GeO_2–SiO_2 samples (Fleming, 1976); it shows large apparent deviations from linearity. The

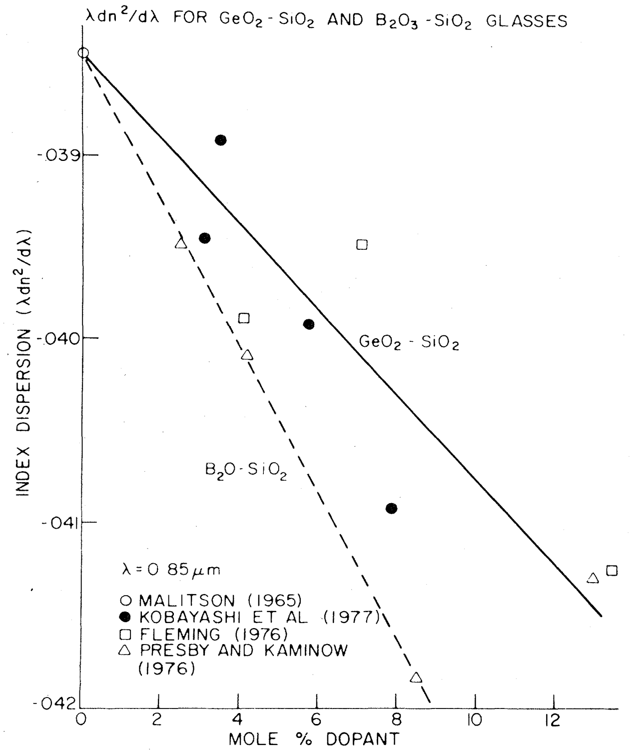

FIG. 12. $\lambda dn^2/d\lambda$ at 0.85 μm vs mol % dopant for GeO_2–SiO_2 preforms (Fleming, 1976; Kobayashi *et al.*, 1977) and B_2O_3–SiO_2 fibers (Presby and Kaminow, 1976). The data do not show evidence of a nonlinear dependence.

Fleming data for $dn^2/d\lambda$ vs n^2 are shown in Fig. 12 along with more recent bulk sample measurements reported by Kobayashi *et al.* (1977). It is not clear whether the spread in data points in Fig. 12 represents random error introduced by the measurement and the derivative calculation or whether it represents real changes in dispersion resulting from variations in sample preparation. At present there are not sufficient data to justify the conclusion that the GeO_2–SiO_2 system exhibits nonlinear dispersion effects.

If nonlinear dispersion corrections are required in optical waveguides, several studies (Arnaud and Fleming, 1976; Arnaud, 1976a; Geckeler, 1978) have shown how to incorporate these effects in profile design.

IV. PERTURBED MULTIMODE WAVEGUIDES

In Secs. II and III, the waveguide has been treated as geometrically perfect. It has been assumed to be straight, to have infinite cladding thickness, cylindrical symmetry, and no variation along the fiber length. Deviations from this ideal geometry can play an important role in waveguide propagation characteristics and in waveguide design considerations. The effects of deviations from the ideal geometry are discussed in this section.

No matter how perfect the fabrication technology, an optical waveguide has a finite cladding thickness and, unless it is very short, undergoes bends of finite radius of curvature.

In the design of the multimode waveguide, it is important to choose the core radius a and relative index difference Δ so that bending losses incurred during normal use do not significantly affect propagation. The cladding must also be designed to be sufficiently thick that the signal propagating in the core is not appreciably attenuated by whatever medium surrounds the cladding. These two topics are addressed in Secs. IV.A and IV.B.

Section IV.C discusses index profile deviations arising from factors such as random fluctuations in the fabrication process, systematic profile perturbations introduced during fabrication, and microscopic random bends produced by external stresses.

All such effects can be described as special cases of a general index profile perturbation, $\delta n^2(r,\theta,z)$. In Sec. IV.C the discussion is subdivided according to whether the perturbation is length independent, length dependent with low spatial frequency so that no mode coupling results, or length dependent with high spatial frequencies producing mode coupling.

A. Curvature loss

A number of researchers have analyzed curvature losses in slab waveguides and in cylindrical step fibers. Solutions to the scalar wave equation can be obtained in the case of the slab waveguide either in terms of Bessel functions (Marcatili, 1969; Marcuse, 1971b) or by using the WKB approximation to solve a conformal transformation of the wave equation (Heiblum and Harris, 1975).

The analysis of the cylindrical fiber is more difficult because of the added geometrical complexity. A result of some of the earlier work (Marcatili and Miller, 1969; Shevchenko, 1973; Gloge, 1972) was the following simple model for bending loss: As a mode propagates through a bend, as a function of radial position the phase velocity $\beta(r)$ must have the form

$$\beta(r)=\beta(0)\frac{R}{r+R}\,, \tag{4.1}$$

where R is the bend radius. This maintains an equiphase plane traverse to the waveguide axis. In the cladding region, the mode field varies as

$$E(r)\propto \exp\left[-\int_a^r \frac{W(r)}{a}\,dr\right], \tag{4.2}$$

where

$$W(r)=a[\beta^2(r)-n_2^2k^2]^{1/2} \tag{4.3}$$

is the generalization of W defined by Eq. (2.13). At a point r_0, defined by the relation

$$\beta(r_0)=n_2k\,, \tag{4.4}$$

the model propagation constant is equal to the value of light freely propagating in the cladding, and radiation occurs.

For a step-index profile, this model leads to a curvature loss (Gloge, 1972)

$$\gamma_c=\frac{2W^2}{\beta a^2}\exp\left[-\frac{2}{3}n_1kR\left(\frac{W^2}{n_1^2k^2a^2}-\frac{2a}{R}\right)^{3/2}\right]. \tag{4.5}$$

In terms of the principal mode number m,

$$W=n_1ka\sqrt{2\Delta}\,[1-(m/M)^2]^{1/2}\,, \tag{4.6}$$

and the curvature loss is

$$\gamma_c = 4n_1k\Delta[1-(m/M)^2]$$
$$\times \exp\left\{-\frac{2}{3}n_1k(2\Delta)^{3/2}R\left[1-\left(\frac{m}{M}\right)^2-\frac{a}{\Delta R}\right]^{3/2}\right\}. \quad (4.7)$$

The factor $n_1k(2\Delta)^{3/2}$ is of the order of 10^2 cm^{-1}. The curvature loss thus varies from completely insignificant values to 10^7 dB/km depending on the mode number. For modes with m approximately equal to or greater than a critical value m_c, defined as

$$\frac{m_c}{M} \approx \left(1-\frac{a}{\Delta R}\right)^{1/2}, \quad (4.8)$$

all power is immediately radiated, while lower-order modes are not significantly affected. The main result of a bend is thus to truncate the waveguide's mode volume at m_c. For a typical waveguide with $a = 25$ μm, $\Delta = 0.01$, and a 5 cm bend radius, the loss is 0.2 dB for a step-index profile.

For a parabolic profile, one can use the appropriate expression for W, that is

$$W_p \approx n_1k\sqrt{2\Delta}\,[1-(m/M)]^{1/2}, \quad (4.9)$$

to find

$$\left(\frac{m_c}{M}\right) \approx 1-\frac{a}{\Delta R}. \quad (4.10)$$

The curvature loss in a parabolic fiber having the same values of a and Δ is thus twice the loss of the step fiber.

By considering bending in a slab waveguide, Heiblum and Harris (1975) showed that under a conformal transformation, the curved guide corresponds to a straight fiber with the transformed index profile

$$\bar{n}(r) = [1+(r/R)\cos\phi]n(r), \quad (4.11)$$

where ϕ is the polar angle measured from the center of the fiber perpendicular to the plane of the bend. From the transformed index profile for a step waveguide, it is clear that the curvature loss can be understood as a tunneling phenomenon. The guided mode tunnels from the core to the caustic created in the cladding by the presence of the bend.

Gloge (1975a) reported that the wave equation for the cylindrical fiber with the transformed index profile [Eq. (4.11)] could be separated in parabolic coordinates and solved by the WKB method. The result is

$$\gamma_c = \frac{\kappa_\nu}{a^2n_2k}\frac{U^2}{V^2}[4W^2+n_2ka\zeta^{4/3}/\bar{R}]^{1/2}$$
$$\times\left(\exp\left\{-\bar{R}\left[\frac{W^2}{(n_2ka)^2}+\left(\frac{\zeta}{\bar{R}}\right)^{2/3}-\frac{2a}{R}\right]^{3/2}\right\}\right), \quad (4.12)$$

where

$$\bar{R} = \tfrac{2}{3}Rn_2k, \quad (4.13)$$

$$\zeta = \pi\begin{cases}\nu+\frac{1}{2} & \text{for even } \nu\\ \nu & \text{for odd } \nu\end{cases}. \quad (4.14)$$

For $\nu = 0$, the exponential factors in Eqs. (4.12) and (4.5) are the same.

Many other approaches have been used to calculate curvature losses with qualitatively similar results (Lewin, 1974; Snyder *et al.*, 1975; Marcuse, 1976a). Using the transformed index profile Marcuse (1976b) showed that the effect of field distortion due to the curvature led to corrections to an earlier result (1976a). Recently Gambling and Matsumura (1977a) observed that near-field patterns are strongly distorted in curved fiber and the resulting mode patterns are well described by a parabolic coordinate system. Gloge's solution, Eq. (4.12), derived from parabolic coordination, must include the effects of field distortion and thus may offer greater accuracy than alternative approaches.

B. Cladding thickness

A low-loss optical waveguide must have a region surrounding the core which provides optical isolation of the core light from the more outlying regions. The term "cladding" is used to denote such a region of low-loss glass immediately adjacent to the core. In accordance with Eq. (2.1), the cladding index is n_2. Its radius shall be designated by b. The cladding can be considered to be surrounded by a third region of complex refractive index

$$n_3 = n_{R3} + in_{I3}. \quad (4.15)$$

If the cladding is too thin, excess losses can occur if the outer region is a region of high loss (large n_{I3}) or if $n_{R3} > n_2$. In the latter case, light from the core can tunnel through the cladding and radiate away.

The theory required to evaluate these effects involves straightforward generalization of the basic theories presented in Sec. II. Numerical calculations for meridional modes ($\nu = 0$) of a step fiber have been discussed by Kuhn (1975) and by Roberts (1975). Using an analysis of meridional rays in a step fiber, Cherin and Murphy (1975) have presented extensive numerical calculations of total transmission loss versus cladding thickness for various fiber parameters.

A general formulation equally applicable to step- and graded-index fibers has been presented by Snyder and Love (1976). They have used a "local plane-wave concept" to determine the power loss from the evanescent field extending into a lossy cladding. The attenuation coefficient is given as

$$\gamma = \frac{1}{Z_p}\frac{n_{I3}n_{R3}k^2}{|q(b)|^2}\exp\left[-2\int_{r_2}^{b}|q(r)|dr\right], \quad (4.16)$$

where $q(r)$ is defined by Eq. (2.42), r_2 is the outer caustic, and Z_p is the distance between successive outer turning points on the ray path. In terms of modes, results of the WKB method (see Appendix) can be used to show

$$Z_p = \frac{\partial\phi_1}{\partial\beta} \quad (4.17)$$

where ϕ_1 is the integral on the right-hand side of Eq. (2.41). For the case of the parabolic profile, Z_p is just one-half of the focal length,

$$Z_p = \frac{\pi a}{\sqrt{2\Delta}}. \quad (4.18)$$

While Eq. (4.16) is appropriate for evaluating the effects of a lossy outer region, even greater losses can occur if $n_{R3} > n_2$. Gloge (1975) has given a result for the step waveguide. Using the WKB approximation, an analogous result can be derived for an arbitrary index profile (see Appendix)

$$\gamma = \frac{1}{Z_p}\left(\frac{k^2 n_{R3}^2 - \beta^2 - \nu^2/b^2}{\beta^2 - k^2 n_2^2 + \nu^2/b^2}\right)^{1/2} \exp\left[-2\int_{r_2}^{b} |q(r)|dr\right]. \tag{4.19}$$

Kashima and Uchida (1977) use the weak guidance approximation to analyze this type of loss in a step waveguide. They develop expressions involving Bessel functions and make numerical calculations of total loss versus wavelength for different waveguide parameters. Their results show that, even for a 15 μm cladding thickness, excess losses on the order of 1 dB/km can result. Using the WKB method, they have recently extended this analysis to graded-index waveguides (Kashima and Uchida, 1978).

C. Index profile perturbations

Fiber curvature and the finite cladding thickness are departures from the ideal geometry which are physically unavoidable in long-length fibers. However, by proper choice of fiber parameters, a, b, and Δ, the multimode waveguide can be designed to reduce these potential loss sources to negligible levels.

A second class of departures from the ideal waveguide geometry are index perturbations introduced by factors such as random fluctuations and systematic deviations characteristic of the fabrication process, or microscopic random bends produced by external stresses. All such effects can be described as special cases of a general index perturbation, $\delta n^2(r,\theta,z)$. Index perturbations can be conveniently divided into three classes according to the perturbation's z dependence.

Define the Fourier-transformed perturbation as

$$\delta\tilde{n}^2(r,\theta,\omega) = \frac{1}{L}\int_0^L dz\, e^{i\omega z}\delta n^2(r,\theta,z). \tag{4.20}$$

The first class consists of the zero-frequency component, which is just the length-averaged perturbation,

$$\delta\tilde{n}^2(r,\theta,0) = \frac{1}{L}\int_0^L dz\,\delta n^2(r,\theta,z). \tag{4.21}$$

Maxwell's equations have lossless guided mode solutions for an arbitrary profile $n^2(r,\theta)$. Thus no zero-frequency perturbation by itself can produce excess loss. In combination with other loss mechanisms, the presence of a zero-frequency perturbation may result in excess loss, but this more complicated interaction between two different effects has not been considered in the literature and will not be discussed further.

The principal interest in zero-frequency perturbations is the effect they have on pulse broadening in fibers with parabolic or other optimal profile shape. Such perturbations are of great importance in waveguide fabrication because these index perturbations must be controlled and limited to obtain waveguides exhibiting low pulse dispersion.

Non-zero-frequency perturbations can be subdivided into two classes according to whether or not they produce mode coupling. It has been shown (Marcuse, 1969a; Snyder, 1970) that coupling of power between modes i and j occurs only if the Fourier-transformed perturbation, defined by Eq. (4.20), contains a frequency component

$$\omega = \beta_i - \beta_j\,. \tag{4.22}$$

Although coupling can occur within a mode group, the more important mode coupling effects which have been observed and extensively studied involve coupling between adjacent mode groups (Gloge, 1972b), that is,

$$|\delta m| = 1\,. \tag{4.23}$$

From Eq. (2.50), one has

$$\delta\beta = \left(\frac{2\alpha}{\alpha+2}\right)^{1/2}\frac{\sqrt{2\Delta}}{a}\left(\frac{m}{M}\right)^{(\alpha-2)/(\alpha+2)} \tag{4.24}$$

for the difference between propagation constants of adjacent mode groups. Equations (4.22) and (4.24) can be used to divide the frequency spectrum of perturbations into a low-frequency region

$$0 < \omega < \left(\frac{2\alpha}{\alpha+2}\right)^{1/2}\frac{\sqrt{2\Delta}}{a}\left(\frac{1}{M}\right)^{(\alpha-2)/(\alpha+2)} \tag{4.25}$$

which does not produce mode coupling and a high-frequency region

$$\omega > \left(\frac{2\alpha}{\alpha+2}\right)^{1/2}\frac{\sqrt{2\Delta}}{a}\left(\frac{1}{M}\right)^{(\alpha-2)/(\alpha+2)} \tag{4.26}$$

which does (Olshansky and Nolan, 1976).

For a parabolic profile, the modal separation is independent of mode number

$$\delta\beta = \frac{\sqrt{2\Delta}}{a}\,, \tag{4.27}$$

while for a step-index profile the separation between propagation constants of adjacent mode groups extends over the range

$$\frac{2}{n_1 k a^2} \leq \delta\beta \leq \frac{2\sqrt{\Delta}}{a}\,. \tag{4.28}$$

For many random perturbations, the power spectrum of the perturbation, defined as

$$P(r,\theta,\omega) = |\delta\tilde{n}^2(r,\theta,\omega)|^2\,, \tag{4.29}$$

is a strongly decreasing function of ω, so that adjacent is dominant over nonadjacent mode coupling. If such is not the case, then frequencies above the ranges of Eqs. (4.27) and (4.28) must be considered.

For a typical waveguide with $a = 30$ μm, $\Delta = 0.01$, and $\lambda = 1$ μm, the coupling frequency for the parabolic profile is 4.7 mm^{-1} and the range for the step-index profile is 0.24 to 6.7 mm^{-1}. In terms of a perturbation period,

$$\Lambda = 2\pi/\omega\,, \tag{4.30}$$

the period is 1.3 mm for the parabolic profile and in the range 0.9–26 mm for the step profile.

Many perturbations introduced during fabrication fall in the low-frequency region. A 10 cm length of preform can produce up to several kilometers of fiber, so that the draw-down ratio is on the order of 10^4. For a perturbation of the preform to fall into the mode coupling region, the perturbed region of the preform must be about 0.1 μm in extent. Most nonuniformities of the preform are believed to extend over much larger distances and thus fall into the low-spatial-frequency, nonmode-coupling class. Similarly, the power spectrum of diameter variations introduced during the draw process also falls into the low-frequency region because of the relatively fast draw speeds, above 0.5 m/s, and the relatively slow mechanical and thermal response of the preform (Runk, 1977). The known index perturbations of the optical waveguide itself thus fall into the low-frequency portion of the power spectrum. The only source of mode coupling which has been observed is from microbending caused by factors such as high winding tension (Keck, 1974; Gardner, 1975) or uneven jacketing (Gloge, 1975b). No mode coupling intrinsic to the waveguide itself has yet been reported.

In the following subsections, all three classes of index perturbations are discussed.

1. Zero-frequency perturbations

For the zero-frequency or length-averaged index perturbation, the principal subject of interest is the effect the averaged index perturbation has on the pulse broadening of fibers with optimal or near optimal profiles.

Two types of perturbations have been analyzed, a localized index deviation (index bump or dip) (Olshansky, 1976a; Khular *et al.*, 1977; Checcacci *et al.*, 1977) and an index profile deviation which is periodic in r (Olshansky, 1976; Arnaud and Mammel, 1976).

The presence of an index dip on the axis is characteristic of fibers made by the inside fabrication process because of dopant volatilization during tube collapse.

Using the Laguerre–Gauss solutions for the parabolic index profile, Eq. (2.36), and first-order perturbation theory, the rms pulse broadening caused by an on-axis index dip can be calculated (Olshansky, 1976a). For a small dip, of index depth δ and rms width w, the excess pulse broadening for a typical multimode waveguide can be expressed as

$$\sigma_{\rm ex} \approx 50\frac{w\delta}{a n_1 \Delta}\ ({\rm ns/km}). \tag{4.31}$$

Khular *et al.* (1977) have used the same calculational approach to study the effect of the index dip on meridional modes ($\nu = 0$). They present curves for the modal delay shift versus V value for different size perturbations.

While only $\nu = 0$ modes propagate substantial power near the axis, a much larger number of modes are affected by a perturbation located off-axis. Perturbations of this type can occur as a result of uncontrolled changes in reactant flows or temperature during preform fabrication. Calculation by first-order perturbation theory shows that the excess pulse broadening increases proportionally as (Olshansky, 1976a)

$$\sigma_{\rm ex} \propto r[1-(r/a)^2] \tag{4.32}$$

for a localized perturbation at position r. For equal modal excitation, the right-hand side of Eq. (4.32) expresses the radial power distribution. The factor $[1-(r/a)^2]$ comes from the parabolic index profile and the factor r is the weighting appropriate to cylindrical geometry.

In the vapor phase oxidation process either glass oxide soot or the glass itself is deposited in layers. This produces a striated refractive index distribution in the preform. The number of stria can vary from ten to several hundred depending on the fabrication conditions and the core radius.

Arnaud and Mammel (1976) have used a time-of-flight method to calculate the rms pulse broadening making a stairlike approximation to the optimal α profile. For $\Delta = 0.02$, the total rms pulse width is found to be 0.08, 0.2, 0.8, and 4.0 ns/km, respectively, for ∞, 40, 20, and 10 stairs.

Olshansky (1976a) has considered the effect of a sinusoidal index perturbation of the form $\sin(2\pi N r/a)$. For a fixed-amplitude perturbation, the largest increase in pulse broadening occurs for

$$N \approx 0.15\,V. \tag{4.33}$$

The effect is found to be two orders of magnitude smaller for $N \geqslant 0.35\,V$. For a typical parabolic waveguide, a sinusoidal perturbation having an amplitude of 0.01Δ produces a maximum excess broadening of 1 ns/km if the period is given by Eq. (4.33).

2. Low-spatial-frequency perturbations

For low-frequency perturbations characterized by Eq.(4.24) the electromagnetic modal fields can adjust adiabatically to the perturbations as they are encountered during propagation. Although the modal delay times will vary along the length of the waveguide, the mean delay shift averages to zero in first-order perturbation theory, except of course for the zero-frequency component.

Low-frequency perturbations do produce excess attenuation of the high-order modes. In regions of the waveguide where perturbations reduce the fiber's guided mode volume, some of the high-order modes adiabatically convert to either leaky modes or radiation modes, and power is lost. Olshansky and Nolan have used a statistical approach to evaluate the excess high-order mode loss resulting from random diameter variations of a step-index (1976) and a parabolic index (1977) profile. A 1% rms diameter variation produces an excess loss of a few tenths dB in the first kilometer of propagation. Other types of low-frequency index profile perturbations will have a similar effect on high-order attenuation.

3. High-spatial-frequency perturbation (mode coupling)

Perturbations having a sufficiently high spatial frequency can satisfy the phase-matching condition [Eq. (4.22)] and cause mode coupling. The theory of mode coupling has been studied extensively in the literature and an excellent summary of this work can be found in Marcuse's text, *Theory of Dielectric Optical Waveguides* (1974a).

The earliest investigations of mode coupling in optical waveguides (Marcuse, 1969a, 1969b) were concerned with the excess losses which can result from the coupling of guided modes to radiation modes. Later Personick (1971) predicted that as a result of random coupling among the guided modes, the pulse broadening would increase as only the square root of the waveguide length, not in proportion to it.

One can understand this result by assuming that the input pulse consists of energy packets which, as a result of perturbations, make random transitions among the modes. Each packet of signals arriving at output will have propagated in a large number of different modes and the arrival times of the packets will be distributed about a mean delay time representing a weighted average of all the modal delay times. The distribution of arrival times about the mean is inversely proportional to the square root of the number of transitions each packet makes. If d is a measure of the coupling strength, the number of transitions is proportional to dL and the width of the distribution about the mean is proportional to $(L/d)^{1/2}$. Thus in the presence of strong mode coupling, the pulse width increases as $(L/d)^{1/2}$.

A number of authors have contributed to the detailed analysis of mode coupling effects. Marcuse worked out mode coupling coefficients for slab waveguides (1969a, 1969b, 1973a). Snyder (1970, 1971) and Marcuse (1973b) derived coupling coefficients for the round fiber.

The coefficient $K_{ij}(z)$ for coupling between modes i and j is given as (Marcuse, 1973b)

$$K_{ij}(z)=\frac{ck\varepsilon_0}{4iP}\int\int r\,dr\,d\theta\,\delta n^2(r,\theta,z)\overline{E}_i^T\cdot\overline{E}_j^T\,, \tag{4.34}$$

where $\overline{E}_i^T$ is the transverse electric field for mode i, ε_0 is the electrical permittivity of the vacuum, and P is a normalization coefficient.

Strong coupling between modes occurs only if the Fourier transform of $K_{ij}(z)$ contains a frequency component ω which satisfies the phase-matching condition (Marcuse, 1969a, b)

$$\omega=\beta_i-\beta_j\,. \tag{4.35}$$

If an index perturbation does cause coupling among the guided modes, Maxwell's equations lead to coupled wave equations for the amplitudes A_i of the electromagnetic fields of modes $i=1\ldots N$. Rowe and Young (1972) showed that in the presence of random perturbations in a two-mode waveguide, one can derive coupled equations for the power P_i in each mode. Marcuse (1972a) generalized this result to N modes and derived the coupled power equations

$$\tau_i\frac{\partial P_i}{\partial t}+\frac{\partial P_i}{\partial z}=\sum_{j=1}^{N}d_{ij}(P_j-P_i)-\gamma_iP_i\,, \tag{4.36}$$

where τ_i and γ_i are, respectively, the delay time and attenuation rate of mode i, and d_{ij} is the coupling coefficient for a transition between modes i and j.

Equation (4.36) expresses the result that in the presence of a random perturbation, the phase information contained in amplitude coefficients A_i can be ignored and only the total power evolution in a mode, $P_i(z,t)$, is of physical interest. The coupled power equations express the intuitive result that the total change in power per unit length in mode i (left-hand side) is equal to the total gain ($\sum d_{ij}P_j$) minus the total loss ($\sum d_{ij}P_i$) in power due to mode coupling, minus the direct attenuation (γ_iP_i) in mode i.

On the basis of observed propagation in optical waveguides, Gloge (1972b) introduced several important simplifications to the analysis of the coupled power equations. First he showed that in a step waveguide the principal mode number m is proportional to the propagation angle θ. Observation of a length-dependent broadening of the far-field pattern in a waveguide excited by a low-numerical-aperture launch beam could then be interpreted as a gradual coupling into higher-order modes. This suggests that the mode coupling is dominated by transitions between adjacent mode groups, and hence

$$d_{mm'}=d_m\delta_{m,m'+1}+d_{m'}\delta_{m',m+1}\,. \tag{4.37}$$

As a further simplification, Gloge approximated the discrete mode spectrum by a modal continuum

$$P_m(z,t)\approx P(m,z,t)\,. \tag{4.38}$$

The result of these approximations is that the coupled power equations can be reduced to a diffusion equation

$$\frac{\partial P}{\partial z}+\tau(m)\frac{\partial P}{\partial t}=-\gamma(m)P+\frac{1}{m}\frac{\partial}{\partial m}md(m)\frac{\partial P}{\partial m}\,, \tag{4.39}$$

where the mode group number m is now treated as a continuous variable. Equation (4.39) can be solved exactly in a number of interesting cases.

Gloge (1972b, 1973) showed that for

$$\gamma(m)=\gamma_0m^2 \tag{4.40}$$

and

$$d(m)=d_0 \tag{4.41}$$

there exist simple closed-form solutions. These solutions express the interesting result that, regardless of the input excitation, after a distance greater than the coupling length, defined as

$$L_c=(\gamma_0d_0)^{-1/2}\,, \tag{4.42}$$

the mode distribution reaches a steady state having an attenuation rate

$$\gamma_s=2(\gamma_0d_0)^{1/2}\,. \tag{4.43}$$

In the time-dependent case, the solutions give the pulse broadening as a function of length.

If in the absence of mode coupling the pulse width increases as

$$\sigma_0(z)=\sigma_0z\,, \tag{4.44}$$

then in the presence of strong mode coupling (when $z\gg L_c$) the pulse broadening is given as

$$\sigma_c(z)=\frac{\sigma_0}{2}\left(\frac{z}{\gamma_s}\right)^{1/2}. \tag{4.45}$$

The features of the transition between the weakly coupled domain ($z\ll L_c$) and the strongly coupled domain ($z\gg L_c$) can be studied in detail from Gloge's solutions.

Marcuse (1973c) extended the analysis to the case of a parabolic index profile with a mode-independent attenuation coefficient. Olshansky (1975) generalized these results to α-class profiles and mode-dependent coupling of the form

$$d(m)=d_0(m)^{-2q}\,. \tag{4.46}$$

All these models have the general feature that, once the power distribution has achieved the steady state, the pulse reduction

$$R=\sigma_c(z)/\sigma_0(z) \tag{4.47}$$

and the excess attenuation due to mode coupling

$$\gamma(z)=\gamma_sz \tag{4.48}$$

satisfy a relationship

$$R^2\gamma = \eta \quad \text{for } z \gg L_c . \tag{4.49}$$

The constant η of Eq. (4.49) is independent of all dimensional parameters and refractive indices. It depends only on the profile shape and mode dependences of the coupling and attenuation coefficients. Equation (4.49) expresses the result that for a given loss penalty γ the pulse broadening is reduced by a factor $(\eta/\gamma)^{1/2}$. It has been proposed (Miller and Personick, 1972; Marcuse, 1974) that by suitably controlling the perturbation, the tradeoff parameter η can be substantially reduced so that large reduction in pulse broadening can be achieved for minimal loss penalty. Such controlled mode coupling has not yet been demonstrated in practice.

4. Microbending losses

Gloge (1972b) proposed that the observed mode coupling in multimode optical fibers was caused by microscopic random bending. This was confirmed by Keck (1974), who induced mode coupling by applying an external stress. For adjacent mode coupling ($|\Delta m| = 1$) in a step waveguide, the coupling coefficient for microbending is (Marcuse, 1969b, 1973b; Gloge, 1972b)

$$d(m) = \frac{4n^2k^2a^2}{\pi^4}\tilde{C}(\delta\beta) \tag{4.50}$$

where $\tilde{C}(\delta\beta)$ is the power spectrum of the fiber's curvature, $C(z)$, and is defined as

$$\tilde{C}(\delta\beta) = \left\langle \left| \frac{1}{\sqrt{L}} \int_0^L dz C(z) e^{i\delta\beta z} \right|^2 \right\rangle . \tag{4.51}$$

The brackets in Eq. (4.51) indicate that an ensemble average is being taken. $\delta\beta$ is the difference between propagation constants of adjacent modes and is given by

$$\delta\beta = \frac{2\sqrt{\Delta}}{a}\left(\frac{m}{M}\right) \tag{4.52}$$

for a step-index waveguide. Marcuse, (1973c) has extended these results to the parabolic index profile.

Fiber microbending under different types of loading (Olshansky, 1975a, b; Gloge, 1975b) has been studied. The results suggest that the curvature power spectrum can be parametrized as

$$\tilde{C}(\Delta\beta) = C_0/(\Delta\beta)^{2p} , \tag{4.53}$$

where $p \gtrsim 1$ in a number of the models studied. This leads to the interesting result (Olshansky, 1975b) that the excess loss due to microbending has the dependence

$$\gamma \sim \frac{1}{\Delta}\left(\frac{a^2}{\Delta}\right)^p . \tag{4.54}$$

Since the study of models suggest $p \geqslant 1$, Eq. (4.54) indicates that microbending loss can be controlled either by reducing the fiber's core radius or increasing its numerical aperture. These trends have been qualitatively verified (Gardner, 1975; Fox, 1977).

D. Multimode *W*-fiber

The name *W*-fiber has been coined (Kawakami and Nishida, 1974, 1975) for the optical waveguide surrounded by two claddings, an inner cladding of index n_2 and thickness $t = b - a$ and an outer cladding of index n_3 where $n_1 > n_3 > n_2$. Although originally proposed for a single-mode fiber, the *W*-fiber design has also been suggested for reducing curvature and microbending losses of multimode fibers (Kawakami *et al.*, 1976).

The modes of the *W*-fiber can be divided into bound modes having

$$n_1k > \beta > n_3k ,$$

and partially bound modes having

$$n_3k > \beta > n_2k .$$

For sufficiently long waveguides the second group of modes can tunnel through the inner cladding and radiate away. This effect has been analyzed theoretically (Maeda and Yamada, 1977) and observed (Tanaka *et al.*, 1977). If the ratio t/λ is large enough, tunneling is negligible and the waveguide behaves as a singly clad fiber with cladding index n_2. For smaller values of t/λ, the partially bound modes radiate quickly and the waveguide behaves as a singly clad fiber with cladding index n_3. In neither case does the *W* fiber appear to offer any advantage over the corresponding singly clad design.

An experimental study of power transmission and splice lossed in *W*-fiber shows the best results were obtained for small n_3-n_2 and large t (Uchida *et al.*, 1978).

V. SINGLE-MODE OPTICAL WAVEGUIDES

Although some of the earliest low-loss optical waveguides propagated only a single mode (Kapron *et al.*, 1970), much of the subsequent research and development activity has concentrated on the properties of multimode waveguides. Because of its large core radius and large numerical aperture, the multimode fiber offers the advantage of efficiently accepting the signal from LED sources, whose reliability is well established and whose cost is low. Even when injection lasers are the chosen optical source, the problem of making low-loss splices or connections between optical fibers is considerably more difficult for the single-mode fiber because of its relatively small core diameter, typically on the order of 5–10 μm.

Recently, progress in the development of injection lasers with long lifetimes (Ladany *et al.*, 1977; Hartman *et al.*, 1977) and the development of techniques for making low-loss single-mode splices (Tynes and Derosier, 1977; Tusuchiya and Hayakayama, 1977) indicates that difficulties originally confronting single-mode communication systems have been greatly ameliorated.

Although these coupling problems are a disadvantage of single-mode systems, the single-mode fiber offers the great advantage that no well-controlled index profile is required to achieve ultrahigh information bandwidths.

Single-mode fibers will inevitably play an important role in future communication systems. Particularly in very high bit rate systems, the single-mode fiber offers bandwidths which can be orders of magnitude greater than will be possible with multimode fibers.

The properties of single-mode waveguides are reviewed in this section.

A. Unperturbed single-mode propagation

1. Weak guidance approximation

The step-index single-mode waveguide is well described by the weak guidance approximation (Gloge, 1971a). With U, W, and V defined by Eqs. (2.12)–(2.15), the propagation constant of the LP_{01} (HE_{11}) mode is

$$\beta = n_2 k (1 + b\Delta) , \tag{5.1}$$

where

$$b = 1 - (U/V)^2 \tag{5.2}$$

and U is determined from the eigenvalue condition, Eq. (2.19). For a given value of V, the corresponding value of b can be determined from either Fig. 2 or Fig. 13.

The fraction of power propagating within the core is a function of V and is given as (Gloge, 1971a)

$$P_{\rm clad}/P_{\rm total} = (U/V)^2 (1 - \kappa_0) \tag{5.3}$$

where κ_0 is defined by Eq. (2.31). This fraction is plotted in Fig. 2.

The unperturbed waveguide supports pure single-mode propagation only in the region

$$0 \leqslant V \leqslant 2.405 . \tag{5.4}$$

However, as can be seen in Fig. 2, for $V \leqslant 1.4$ less than half of the modal power propagates in the core. As a result, single-mode waveguides having small V values are subject to high losses caused by factors such as curvature, limited cladding thickness, or microbending.

On the other hand, in the region above the single-mode cutoff, the next set of modes (LP_{11}) have a large fraction of their power propagating in the cladding. For example, at $V = 2.7$ about 50% of the LP_{11} power is in the cladding. Thus, in the region above cutoff, the LP_{11} modes are susceptible to various loss mechanisms (Gambling *et al.*, 1977b; Tasker *et al.*, 1977) and only the LP_{01} mode can successfully propagate.

The properties of graded-index single-mode waveguides have been partially explored. Marcuse (1978) has shown that for power-law profiles the waveguide's fields can be well approximated by a Gaussian function.

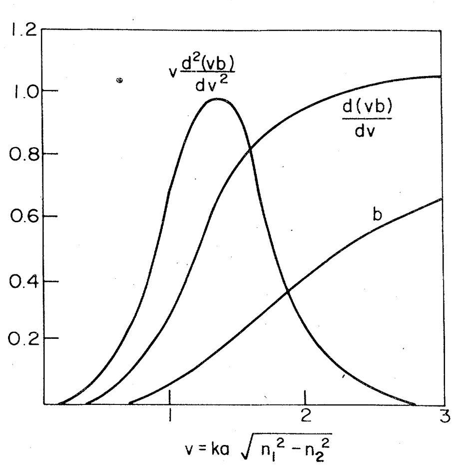

FIG. 13. Functions characterizing single-mode propagation are plotted vs V (after Gloge, 1971b).

This approximation will simplify the analysis of the effects of perturbations on graded-index single-mode propagation.

For power-law profiles, Gambling, Payne, and Matsumura (1977) have analyzed the shift in cutoff value as a function of the profile. For $\alpha = 2$, they find $V = 3.50$, in agreement with an earlier result of Dil and Blok (1973).

Because of the diffraction-limited nature of single-mode propagation, the conventional near-field and far-field measurements, which are used successfully to determine a and Δ for multimode waveguides, do not directly provide a measurement of the single-mode waveguide's parameters. Gambling and Matsumura (1977a) have shown how a more detailed analysis of the far-field pattern can yield a measure of a, Δ, and V. Timmerman (1977) has provided a simplified closed-form expression for the single-mode far-field pattern which is useful in analyzing the measurement.

2. Pulse dispersion

The rms pulse broadening of a single-mode waveguide is given as

$$\sigma_{\rm tot} = \frac{L}{c} \sigma_\lambda \frac{d}{d\lambda}\left(\frac{d\beta}{dk}\right) , \tag{5.5}$$

where σ_λ is the source spectral linewidth. The pulse broadening can be written as the sum of a pure material dispersion term and a waveguide-related term (Gloge, 1971b; Kapron and Keck, 1971; Dyott and Stern, 1971),

$$\sigma_{\rm tot} = |\sigma_{\rm mat} + \sigma_{\rm wg}| , \tag{5.6}$$

where

$$\sigma_{\rm mat} = \frac{L}{c} \sigma_\lambda \lambda \frac{d^2 n}{d\lambda^2} \tag{5.7}$$

and (Gloge, 1971b)

$$\sigma_{\rm wg} = \frac{L}{c} \frac{\sigma_\lambda}{\lambda} n_1 \Delta V \frac{d^2(Vb)}{dV^2} . \tag{5.8}$$

The factor $Vd^2(Vb)/dV^2$ is shown in Fig. 13.

In the spectral region 0.8–0.9 μm, the material dispersion proportionality factors, $\lambda d^2n/cd\lambda^2$, vary from 106 to 66 ps km^{-1} nm^{-1} for fused silica. The waveguide term can be neglected in this spectral region.

For the high-silica compositions presently being used, the material dispersion term has a zero in the range 1.25–1.35 μm. The exact location of the zero for different compositions has been discussed in Sec. III B 1. The zero in the total pulse dispersion is shifted slightly to longer wavelengths by the waveguide term of Eq. (5.6) (Kapron and Keck, 1971). The shift can be as large as 100 nm for waveguides with large Δ values (Kapron and Keck, 1971; Cohen and Lin, 1977).

The observation of the zero dispersion point at 1.27 μm in a B_2O_3–SiO_2 single-mode waveguide has been reported by Cohen and Lin (1977).

At the zero dispersion point $d\tau/d\lambda$ vanishes and the actual pulse broadening is determined by higher outer terms. Kapron (1977) has made this analysis for a SiO_2 waveguide and found that the minimum pulse dispersion is 2.5×10^{-2} ps km^{-1} nm^{-2}. The carrier frequency limit is 2×10^{-3} ps.

B. Perturbed single-mode propagation

In designing single-mode fibers, one should select the parameters a, Δ, and V so as to make the spot size large enough to obtain low splicing and interconnection losses, and yet small enough that curvature and microbending losses are negligible. The low-loss cladding surrounding the core should be sufficiently thick that losses due to either an absorptive outer layer or a high-index outer layer ($n_3 > n_2$) are negligible. These topics are discussed below.

1. Single-mode curvature loss

As is true for the curvature loss of multimode fibers, the theory is quite difficult, and a large number of researchers have derived qualitatively similar results for the single-mode curvature loss. Many of the calculations approximate the fields of the curved fiber by the fields of the straight fiber (Shevchenko, 1973; Lewin, 1974; Arnaud, 1974; Snyder *et al.*, 1975; Marcuse, 1976b). The modal fields, however, are considerably distorted by the bend (Kuester and Chang, 1975; Marcuse, 1976c; Miyagi and Yip, 1977) and this leads to increased loss for the LP_{01} mode. The use of parabolic coordinates (Gloge, 1975) appears to be the most natural description of the distorted fields since it gives a qualitatively good description of the observed fields of a bent fiber (Gambling and Matsumura, 1977a).

In addition to the radiation from a bend of constant curvature, there is a transition region between the straight and bent fiber (Miyagi and Yip, 1977). In the transition region, the radiation emitted in the transverse direction is in the form of discrete beams (Gambling, Payne, and Matsumura, 1976). The radiation from the transition region has been analyzed in terms of coupling between the LP_{01} mode and the LP_{11} leaky mode (Sammut, 1977).

As a practical matter, curvature losses are predicted to be negligible for bend radii encountered in a typical communication system. From the results of Gloge (1975), a single-mode fiber with $a \leqslant 5\ \mu$m and $V \geqslant 2.0$ is predicted to have less than 1 dB/km bend loss for curvature radii greater than 2.5 cm. The results of Marcuse (1976c) yield a completely negligible loss for $a \leqslant 5\ \mu$m, $V \geqslant 2.4$, and $R > 2.5$ cm.

2. Single-mode microbending loss

A more serious practical consideration in single-mode propagation is the magnitude of the microbending losses. For a fixed V value and source wavelength, the single-mode microbending losses increase as a^{2+4p}, where p is the parameter characterizing the curvature power spectrum defined in Eq. (4.53). For this class of power spectra, the microbending losses have the form (Petermann, 1976a, 1976b; Marcuse, 1976a; Olshansky, 1976c)

$$\gamma = \frac{C_0 G(V,p)}{\Delta (n_2 k \Delta)^{2p}}, \tag{5.9}$$

where G is a factor depending only on V and p, and C_0 is the coefficient of the power spectrum. There is not complete agreement on the value of $G(V,p)$ but it decreases with V and is of order unity for $V = 2.4$. For a curvature power spectrum having $p \approx 1-2$, the single-mode microbending loss is about the same as that of a multimode fiber having $a = 30\ \mu$ and $\Delta = 0.01$ if the single-mode fiber's core radius is 4–5 μm.

Several researchers (Petermann, 1976a, 1976b; Marcuse, 1977; Gambling, Matsumura, and Cowley, 1978) have emphasized that it is the spot size of the LP_{01} mode, not the core radius, which is the important parameter controlling splice losses. The spot size w_0, defined as

$$w_0^2 = \int_0^\infty E^2 r^3 dr \Big/ \int_0^\infty E^2 r\, dr, \tag{5.10}$$

is given by (Gambling and Matsumura, 1977b)

$$w_0 = a\left[\frac{2}{3}\left(\frac{J_0(U)}{UJ_1(U)} + \frac{1}{2} + W^{-2} - U^{-2}\right)\right]^{1/2}. \tag{5.11}$$

In the range $1.6 \leqslant V \leqslant 2.6$, Eq. (5.11) can be approximated as either

$$w_0 = 1.9\, a/V \tag{5.12}$$

or

$$w_0 = \frac{1.9}{2\pi} \frac{\lambda}{(2n_1\Delta)^{1/2}}. \tag{5.13}$$

Although spot size is proportional to core radius if V is fixed, Eq. (5.13) makes it clear that the spot size is more directly controlled by λ and Δ.

Using Eq. (5.9) and Eq. (5.13), at fixed V, we find that the microbending losses are proportional to

$$\gamma \propto w_0^{(2+4p)} k^{(2+2p)}. \tag{5.14}$$

Equation (5.14) shows that, for constant splice loss (fixed w_0) and fixed V, microbending losses will decrease strongly with wavelength. This result can be qualitatively understood from Eq. (5.13). If the spot size is fixed, transmission at longer wavelengths permits higher Δ. This gives tighter confinement and lower microbending loss.

3. Cladding thickness

If the cladding is surrounded by a medium of index n_3 and loss coefficient γ_3, two types of loss mechanisms can occur.

For $kn_3 > \beta$, the outer layer acts as a mode stripper and light is very rapidly lost unless the cladding is quite thick. Gloge (1975) has analyzed this case and his result can be expressed as

$$\gamma = \frac{[(kn_3)^2 - \beta^2]^{1/2}}{n_1 ka} \kappa_0 (U/V)^2 \exp\left(-\frac{2Wt}{a}\right), \tag{5.15}$$

where $t = b - a$ is the cladding thickness.

If $kn_3 < \beta$, but the outer medium is lossy, the LP_{01} absorption loss is given by the fraction of power propagating in the outer layer multiplied by its loss coefficient

$$\gamma = \gamma_3 \kappa_0 (U/V)^2 \exp(-2Wt/a). \tag{5.16}$$

If the difference $(n_3 - \beta/k)$ is 10^{-4}, the loss predicted by Eq. (5.15) is equivalent to that of Eq. (5.16) with $\gamma_3 \approx 10^7$ dB/km. Thus the mode-stripping effect of a slightly higher index outer layer is much more troublesome than that of a low-index ($kn_3 < \beta$) but lossy outer layer. Gloge (1975) has estimated that in the former case $t/a \approx 8$ is required for a typical single-mode waveguide if the excess loss is to be limited to less than 1 dB/km.

C. Single-mode W-fiber

A doubly clad single-mode fiber, called a W-fiber, has been proposed (Kawakami and Nishida, 1974, 1975) as a method of reducing both bending losses and pulse dispersion. The W-fiber has a core of radius a and index n_1, an inner cladding of thickness $t=b-a$ and index n_2, and an outer cladding of index n_3, such that

$$n_1 > n_3 > n_2 . \tag{5.17}$$

The core region supports more than one mode but the index n_3 is chosen great enough so that all modes but the LP_{01} tunnel through the inner cladding and do not contribute to the transmitted signal.

1. Microbending loss

The LP_{01} mode of the W-fiber is more tightly confined than the LP_{01} mode of a singly clad fiber of core radius a and cladding index n_3. It has lower microbending loss, but also a smaller spot size. Since the small spot size leads to higher splicing losses, a meaningful comparison can be made only between singly and doubly clad fibers with the same spot size.

Petermann and Storm (1976) find the microbending losses of the W-fiber are comparable to or greater than the losses of singly clad fibers with equal spot size. The W-fiber's microbending loss can be qualitatively understood using the analysis of single-mode spot size made by Gambling and Matsumura (1977b). Taking

$$V = ka(n_1^2 - n_2^2)^{1/2} \tag{5.18}$$

for the W-fiber, their results show that a large core radius is needed to obtain a spot size equivalent to that of a normal single-mode fiber. For a large core radius, the mode spacing between the LP_{01} and LP_{11} modes is small, and increased mode coupling losses result.

2. Anomalous dispersion

At wavelengths shorter than the zero dispersion point, the material dispersion σ_{mat} and the waveguide dispersion σ_{wg} of the singly clad fiber have the same sign. In the W-fiber, they have the opposite sign so that cancellation between them is possible (Kawakami and Nishida, 1974, 1975). However, the index difference $(n_1-n_3)/n_1$ must be on the order of 1% and the difference $(n_1-n_2)/n_1$ must be even larger for full cancellation (Kawakami *et al.*, 1976). Such a waveguide design seems impractical because of the small core size and large index differences required.

ACKNOWLEDGMENTS

The author is very grateful to Dr. D. B. Keck, Dr. R. D. Maurer, and Dr. P. C. Schultz for many helpful suggestions.

APPENDIX: WKB SOLUTION FOR GRADED-INDEX OPTICAL WAVEGUIDES

The WKB solution for graded-index optical waveguides is summarized below. If

$$q(r) = |k^2 n^2(r) - \beta^2 - \nu^2/r^2|^{1/2} \tag{A1}$$

and the caustics r_1 and r_2 are defined as

$$q(r_1) = q(r_2) = 0 , \tag{A2}$$

then in the core the transverse electromagnetic fields have the radial dependence

$$R(r) = \frac{1}{(xq)^{1/2}} \exp\left(-\int_r^{r_1} q\,dr\right), \quad r \le r_1 , \tag{A3}$$

$$R(r) = \frac{2}{(xq)^{1/2}} \cos\left(\int_{r_1}^{r} q\,dr - \frac{\pi}{4}\right), \quad r_1 < r < r_2 , \tag{A4}$$

$$R(r) = \frac{1}{(xq)^{1/2}} \left[\sin\phi_1 \exp\left(-\int_{r_2}^{r} q\,dr\right) + 2\cos\phi_1 \times \exp\left(+\int_{r_2}^{r} q\,dr\right)\right], \quad r_2 < r < a , \tag{A5}$$

where

$$\phi_1 = \int_{r_1}^{r_2} q\,dr . \tag{A6}$$

The field solutions for $r > a$ vary according to the problem under consideration.

1. Cladding neglected

If the presence of the cladding is neglected (Gloge and Marcatili, 1973; Olshansky and Keck, 1976), then Eq. (A5) is taken as valid for all $r \ge r_2$. The requirement that $R(r)$ be zero at infinity gives

$$\cos\phi_1 = 0 \tag{A7}$$

or

$$\phi_1 = (\mu + \tfrac{1}{2})\pi . \tag{A8}$$

The solution of this equation is discussed in Sec. II.

2. Infinite cladding

The cladding can be taken into account by writing the cladding fields as (Olshansky, 1977)

$$R(r) = \frac{1}{(x\bar{q})^{1/2}} \exp\left(-\int_a^r \bar{q}\,dr\right), \tag{A9}$$

where

$$\bar{q} = |k^2 n_2^2 - \beta^2 - \nu^2/r^2|^{1/2}. \tag{A10}$$

Requiring that $R(r)$ and dR/dr be continuous at $r=a$ gives the eigenvalue equation

$$\cos\phi_1 = \delta , \tag{A11}$$

where

$$\delta = \frac{1}{16} \frac{k^2}{\bar{q}(a)^3} \frac{dn^2}{dr}\bigg|_{r=a} \exp(-2\phi_2) \tag{A12}$$

and

$$\phi_2 = \int_{r_2}^{a} q\,dr . \tag{A13}$$

Since the right-hand side of (A12) is small, the eigenvalue equation can be solved as a Taylor expansion about $\delta = 0$. This gives the result

$$\delta\beta = -\frac{\delta}{\partial\phi_1/\partial\beta} . \tag{A14}$$

The shift in delay time caused by the cladding can be calculated from (A14).

3. Finite cladding

If the low-loss cladding extends only to radius b, and for $r > b$ there is a second medium of complex index n_3, two important cases need to be considered.

(a) $\mathrm{Re}n_3 > n_2$ and $\mathrm{Im}n_3 = 0$

In the cladding region, the fields are given as

$$R(r) = \frac{1}{(r\bar{q})^{1/2}}\left[A\exp\left(-\int_a^r \bar{q}\,dr\right) + B\exp\left(\int_a^r \bar{q}\,dr\right)\right] \quad a \le r \le b\,, \tag{A15}$$

and the outer region as

$$R(r) = \frac{1}{(r\bar{\bar{q}})^{1/2}}\,C\exp\left(i\int_b^r \bar{\bar{q}}\,dr\right), \quad b \ge r\,, \tag{A16}$$

where

$$\bar{\bar{q}} = |k^2 n_3^2 - \beta^2 - \nu^2/r^2|^{1/2}\,. \tag{A17}$$

(b) $\mathrm{Re}n_3 = n_2$ and $\mathrm{Im}n_3 \ne 0$

In this case of a low-index, lossy outer medium, the cladding field is still given as (A15) and in the outer region

$$R(r) = \frac{1}{(r\bar{\bar{q}})^{1/2}}\exp\left(-\int_b^r \bar{\bar{q}}\,dr\right). \quad b < r\,. \tag{A18}$$

The boundary conditions at $r = a$ and $r = b$ lead to an eigenvalue equation of the form

$$\cos\phi_1 = \mathrm{Re}\delta + i\,\mathrm{Im}\delta\,. \tag{A19}$$

Again making a Taylor series expansion one finds the attenuation coefficient is

$$\gamma = 2\,\mathrm{Im}\delta\beta = -\frac{2\,\mathrm{Im}\delta}{\partial\phi_1/\partial\beta}\,. \tag{A20}$$

Expressions for γ are given by Eqs. (4.16) and (4.19).

REFERENCES

Adams, M. J., D. N. Payne, and F. M. E. Sladen, 1975, Electron. Lett. **11**, 238.
Adams, M. J., D. N. Payne, and F. M. E. Sladen, 1976, Electron. Lett. **12**, 281.
Arnaud, J. A., 1974a, Electron. Lett. **11**, 8.
Arnaud, J. A., 1974b, Bell Syst. Tech. J. **53**, 1379.
Arnaud, J. A., 1974c, Bell Syst. Tech. J. **53**, 1599.
Arnaud, J. A., 1975, Electron. Lett. **11**, 447.
Arnaud, J. A., 1976a, Electron. Lett. **12**, 654.
Arnaud, J. A., 1976b, *Beam and Fiber Optics* (Academic, New York).
Arnaud, J. A., and R. M. Derosier, 1976, Bell Syst. Tech. J. **55**, 1489.
Arnaud, J. A., and J. W. Fleming, 1976, Electron. Lett. **12**, 167.
Arnaud, J. A., and W. Mammel, 1976, Electron. Lett. **12**, 6.
Bagley, B. G., E. M. Vogel, W. G. French, G. A. Pasteur, J. N. Gan, and J. Tauc, 1976, J. Non-Cryst. Solids **22**, 423.
Bates, C. W., Jr., 1976, Appl. Opt. **15**, 2976.
Bates, T., 1962, in *Modern Aspects of the Vitreous State*, edited by J. D. Mackenzie, Vol. 2 (Butterworth, Washington, D.C.).
Born, M., and E. Wolf, 1970, *Principles of Optics*, 4th ed. (Pergamon, Oxford), p. 10.
Checcacci, P. F., R. Falciai, and A. M. Sheggi, 1977, Electron. Lett. **13**, 379.
Cherin, A. H., and E. J. Murphy, 1975, Bell Syst. Tech. J. **54**, 1975.
Cohen, L. G., 1975, Appl. Opt. **14**, 1351.
Cohen, L. G., 1976, Appl. Opt. **15**, 1808.
Cohen, L. G., and C. Lin, 1977, Appl. Opt. **16**, 3137.
Conradi, J., F. P. Kapron, and J. C. Dyment, 1978, IEEE Trans. Electron Devices ED-25, 180.
Cook, J. S., 1977, Bell Syst. Tech. J. **56**, 719.
Costa, B., and B. Sordo, 1976, in *Proceedings of the Second European Conference on Optical Fibre Communication*, Paris (Comité du Colloque International sur le Transmission par Fibres Optiques, Paris), p. 81.
DiDomenico, M., Jr., 1972, Appl. Opt. **11**, 652.
Dil, J. G., and H. Blok, 1973, Opto-Electron. **5**, 415.
DiVita, P., and R. Vannuci, 1976, Appl. Opt. **15**, 2765.
Dyott, R. B., and J. R. Stern, 1971, Electron. Lett. **7**, 82.
Fabelinskii, I. L., 1968, *Molecular Scattering of Light* (Plenum, New York).
Fleming, J. W., 1976, J. Am. Ceram. Soc. **54**, 503.
Fox, M., 1977, Microwaves, Optics and Acoustics **1**, 133.
French, W. G., J. P. MacChesney, P. B. O'Connor, and G. W. Tasker, 1974, Bell Syst. Tech. J. **53**, 951.
French, W. G., A. D. Pearson, G. W. Tasker, and J. B. MacChesney, 1973, Appl. Phys. Lett. **23**, 338.
French, W. G., G. W. Tasker, and J. R. Simpson, 1976, Appl. Opt. **15**, 1803.
Gambling, W. A., and H. Matsumura, 1977a, Electron. Lett. **13**, 532.
Gambling, W. A., and H. Matsumura, 1977b, Electron. Lett. **13**, 691.
Gambling, W. A., H. Matsumura, and A. G. Cowley, 1978, Electron. Lett. **14**, 54.
Gambling, W. A., D. N. Payne, C. R. Hammond, and S. R. Norman, 1976, Proc. Inst. Electr. Eng. **123**, 570.
Gambling, W. A., D. N. Payne, and H. Matsumura, 1976, Electron. Lett. **12**, 567.
Gambling, W. A., D. N. Payne, and H. Matsumura, 1977, Electron. Lett. **13**, 139.
Gambling, W. A., D. N. Payne, H. Matsumura, and R. B. Dyott, 1977a, Microwaves, Optics and Acoustics **1**, 13.
Gambling, W. A., D. N. Payne, H. Matsumura, and S. R. Norman, 1977b, Electron. Lett. **13**, 133.
Gardner, W. B., 1975, Bell Syst. Tech. J. **54**, 457.
Geckler, S., 1976, Electron. Lett. **16**, 29.
Geckler, S., 1978, Appl. Opt. **17**, 1023.
Geittner, P., D. Küppers, and H. Lydtin, 1976, Appl. Phys. Lett. **28**, 645.
Gibbons, G., 1977, in *Proceedings of the Topical Meeting on Optical Fiber Transmission II*, Williamsburg, Va., WB1 (Optical Society of America, Washington, D.C.).
Gloge, D., 1971a, Appl. Opt. **10**, 2252.
Gloge, D., 1971b, Appl. Opt. **10**, 2442.
Gloge, D., 1972a, Appl. Opt. **11**, 2506.
Gloge, D., 1972b, Bell Syst. Tech. J. **51**, 1767.
Gloge, D., 1973, Bell Syst. Tech. J. **52**, 801.
Gloge, D., 1975a, IEEE Trans. Microwave Theory Tech. MTT-23, 106.
Gloge, D., 1975b, Bell Syst. Tech. J. **54**, 245.
Gloge, D., and E. A. J. Marcatili, 1973, Bell Syst. Tech. J. **52**, 1563.
Gupta, P. K., J. Schroeder, I. D. Aggarwal, and P. B. Macedo, 1974, in *Proceedings of the Symposium on Optical and Acoustic Micro-Electronics*, New York (Polytechnic, Brooklyn), p. 175.
Hammond, C. R., and S. R. Norman, 1977, Opt. and Quant. Electron. **9**, 399.
Hartman, R. L., N. E. Schumaker, and R. W. Dixon, 1977, Appl. Phys. Lett. **31**, 756.
Hashimoto, M., 1976, IEEE Trans. Microwave Theory Tech. MTT-24, 404.
Heiblum, M., and J. H. Harris, 1975, IEEE J. Quantum Electron. QE-11, 75.
Hersee, S. D., and R. C. Goodfellow, 1976, in *Proceedings of the Second European Conference on Optical Fibre Communi-*

cation, Paris (Comité du Colloque International sur le Transmission par Fibres Optiques, Paris), p. 213.
Horiguchi, M., 1978 (private communication).
Horiguchi, M., and H. Osanai, 1976, Electron. Lett. **12**, 310.
Ikeda, K., H. Kan, E. Oomura, K. Matsui, M. Ishii, and W. Susaki, 1977, in *Proceedings of the International Conference on Integrated Optics and Optical Fiber Communication*, Tokyo (Institute of Electronics and Communication Engineers of Japan, Tokyo), p. 77.
Ikeda, K., and M. Yoshiyagawa, 1976, in *Proceedings of the Second European Conference on Optical Fibre Communication*, Paris (Comité du Colloque International sur le Transmission par Fibres Optiques, Paris), p. 27.
Ishikawa, S., K. Furuya, and Y. Suematsu, 1977, in *Proceedings of the International Conference on Integrated Optics and Optical Fiber Communication*, Tokyo (Institute of Electronics and Communication Engineers of Japan, Tokyo), p. 427.
Izawa, T., S. Kobayashi, S. Sudo, and F. Hanawa, 1977, in *Proceedings of the International Conference on Integrated Optics and Optical Fiber Communication*, Tokyo (Institute of Electronics and Communication Engineers of Japan, Tokyo), p. 375.
Izawa, T., N. Shibata, and A. Takeda, 1977, Appl. Phys. Lett. **31**, 33.
Jaeger, R. E., J. B. MacChesney, and T. J. Miller, 1978, Bell Syst. Tech. J. **57**, 205.
Kaiser, P., 1974, J. Opt. Soc. Am. **64**, 475.
Kaiser, P., A. R. Tynes, H. W. Astle, A. D. Pearson, W. G. French, A. E. Jaeger, and A. H. Cherin, 1973, J. Opt. Soc. Am. **63**, 1141.
Kaminow, I. P., and H. M. Presby, 1977, Appl. Opt. **16**, 108.
Kao, K. C., and G. A. Hockam, 1966, Proc. Inst. Electr. Eng. **113**, 1151.
Kapany, N. S., and J. J. Burke, 1972, *Optical Waveguides* (Academic, New York).
Kapron, F. P., 1977, Electron. Lett. **13**, 96.
Kapron, F. P., and D. B. Keck, 1971, Appl. Opt. **10**, 1519.
Kapron, F. P., D. B. Keck, and R. D. Maurer, 1970, Appl. Phys. Lett. **17**, 423.
Kashima, N., and N. Uchida, 1977, Appl. Opt. **16**, 1038.
Kashima, N., and N. Uchida, 1978, Appl. Opt. **17**, 1199.
Kato, D., 1973, Appl. Phys. Lett. **22**, 3.
Katsuyama, T., T. Suganuma, K. Ishida, and G. Toda, 1977, Opt. Commun. **21**, 182.
Kawakami, S., 1976, Appl. Opt. **15**, 2778.
Kawakami, S., and S. Nishida, 1974, Electron. Lett. **10**, 38.
Kawakami, S., and S. Nishida, 1975, IEEE J. Quantum Electron. **QE-11**, 130.
Kawakami, S., S. Nishida, and M. Sumi, 1976, Proc. Inst. Electr. Eng. **123**, 586.
Kawakami, S., and T. Nishizawa, 1968, IEEE Trans. Microwave Theory Tech. **MTT-16**, 814.
Keck, D. B., 1974, Proc. IEEE **62**, 649.
Keck, D. B., and R. Bouille, 1978, Opt. Commun. **25**, 43.
Keck, D. B., R. D. Maurer, and P. C. Schultz, 1973, Appl. Phys. Lett. **22**, 307.
Keck, D. B., and P. C. Schultz, 1973, U. S. Pat. 3,711,262.
Keck, D. B., P. C. Schultz, and F. Zimar, 1972, Appl. Phys. Lett. **21**, 215.
Keck, D. B., P. C. Schultz, and F. Zimar, 1973, U. S. Pat. 3,737,292.
Khular, E., A. Kumar, A. K. Ghatak, 1977, Opt. Commun. **23**, 263.
Kobayashi, S., S. Shibata, N. Shibata, and T. Izawa, 1977, in *Proceedings of the International Conference on Integrated Optics and Optical Fiber Communications*, Tokyo (Institute of Electronics and Communication Engineers of Japan, Tokyo), p. 309.
Koenigs, J., D. Küppers, H. Lydtin, and H. Wilson, 1975, in *Proceedings of the Fifth International Conference on Chemical Vapor Deposition*, (Electrochemical Society, New York), p. 270.
Koizumi, K., Y. Ikeda, I. Kitano, M. Furukawa, and T. Sumimoto, 1974, Appl. Opt. **13**, 255.
Kuhn, M. H., 1975a, Archiv Elektron. Ubertrangungstechnik. **29**, 201.
Kuhn, M. H., 1975b, Archiv Elektron. Ubertrangungstechnik. **29**, 353.
Kuhn, M. H., 1975c, Archiv Elektron. Ubertrangungstechnik. **29**, 400.
Kuster, E. F., and D. C. Chang, 1975, IEEE J. Quantum Electron. **QE-11**, 903.
Laberge, N. L., P. K. Gupta, and P. B. Macedo, 1975, J. Non-Cryst. Solids **17**, 61.
Laberge, N. L., V. V. Vasilescu, C. J. Montrose, and P. B. Macedo, 1973, J. Am. Ceram. Soc. **56**, 506.
Ladany, I., M. Ettenberg, H. F. Lockwood, and H. Kressel, 1977, Appl. Phys. Lett. **30**, 87.
Landau, L. D., and E. M. Lifshitz, 1958, *Statistical Physics* (Addison-Wesley, Reading, Mass.).
Langer, R. E., 1949, Trans. Am. Math. Soc. **67**, 461.
Lewin, L., 1974, IEEE Trans. Microwave Theory Tech. **MTT-22**, 718.
Lin, C., L. G. Cohen, W. G. French, and V. A. Foertmayer, 1978, Electron. Lett. **14**, 170.
Love, J. D., and C. Pask, 1976, Electron. Lett. **12**, 254.
Luther-Davies, B., D. N. Payne, and W. A. Gambling, 1975, Opt. Commun. **13**, 84.
MacChesney, J. B., P. B. O'Connor, and H. M. Presby, 1974, Proc. IEEE **62**, 1280.
Maeda, M., and S. Yamada, 1977, Appl. Opt. **16**, 2199.
Malitson, I. H., 1965, J. Opt. Soc. Am. **55**, 1205.
Marcatili, E. A. J., 1969, Bell Syst. Tech. J. **48**, 2103.
Marcatili, E. A. J., 1977, Bell Syst. Tech. J. **56**, 49.
Marcatili, E. A. J., and S. E. Miller, 1969, Bell Syst. Tech. J. **48**, 2161.
Marcuse, D., 1969a, Bell Syst. Tech. J. **48**, 3187.
Marcuse, D., 1969b, Bell Syst. Tech. J. **48**, 3233.
Marcuse, D., 1971a, Bell Syst. Tech. J. **50**, 1791.
Marcuse, D., 1971b, Bell Syst. Tech. J. **50**, 2551.
Marcuse, D., 1972a, Bell Syst. Tech. J. **51**, 229.
Marcuse, D., 1972b, Bell Syst. Tech. J. **51**, 1199.
Marcuse, D., 1972c, *Light Transmission Optics* (Van Nostrand, New York).
Marcuse, D., 1973a, Bell Syst. Tech. J. **52**, 63.
Marcuse, D., 1973b, Bell Syst. Tech. J. **52**, 817.
Marcuse, D., 1973c, Bell Syst. Tech. J. **52**, 1423.
Marcuse, D., 1974a, *Theory of Dielectric Optical Waveguides* (Academic, New York).
Marcuse, D., 1974b, Bell Syst. Tech. J. **53**, 1795.
Marcuse, D., 1976a, Bell Syst. Tech. J. **55**, 937.
Marcuse, D., 1976b, J. Opt. Soc. Am. **66**, 216.
Marcuse, D., 1976c, J. Opt. Soc. Am. **66**, 311.
Marcuse, D., 1977, Bell Syst. Tech. J. **56**, 703.
Marcuse, D., 1978, J. Opt. Soc. Am. , 103.
Maurer, R. D., 1973, Proc. IEEE **61**, 452.
Maurer, R. D., 1976, Proc. Inst. Electr. Eng. **123**, 581.
Maurer, R. D., and P. C. Schultz, 1972, U. S. Pat. 3,659,915.
Maurer, R. D., and P. C. Schultz, 1975, U. S. Pat. 3,884,550.
Maurer, S. J., and L. B. Felsen, 1970, IEEE Trans. Microwave Theory Tech. **MTT-18**, 584.
McKelvey, R. W., 1959, Trans. Am. Math. Soc. **91**, 410.
Miller, S. E., 1965, Bell Syst. Tech. J. **44**, 2017.
Miller, S. E., E. A. J. Marcatili, and T. Li, 1973, Proc. IEEE **61**, 1703.
Miller, S. E., and S. D. Personick, 1972, U. S. Pat. 3,687,514.
Misugi, T., and H. Takanashi, 1977, in *Proceedings of the International Conference on Integrated Optics and Optical Communication*, Tokyo (Institute of Electronics and Communication Engineers of Japan, Tokyo), p. 53.
Mita, H., S. Matsushita, T. Yanase, and H. Nomura, 1977, Electron. Lett. **13**, 55.
Miyagi, M., and G. L. Yip, 1977, Opt. Quant. Electron. **9**, 51.
Nakamura, M., K. Aiki, J. Umeda, N. Chinone, R. Ito, and H. Nakashima, 1977, in *Proceedings of the International Conference on Integrated Optics and Optical Fiber Communication*, Tokyo (Institute of Electronics and Communication Engineers of Japan, Tokyo), p. 83.
Newns, G. R., K. J. Beales, and C. R. Day, 1977, in *Proceedings of the International Conference on Integrated Optics and Optical Fiber Communication*, Osaka (Institute of Electronics and Communication Engineers of Japan, Tokyo), p. 609.

O'Connor, P. B., J. B. MacChesney, and F. V. DiMarcello, 1976, in *Proceedings of the Second European Conference on Optical Fibre Communication*, Paris (Comité du Colloque International sur le Transmission par Fibres Optiques, Paris), p. 55.
O'Connor, P. B., J. B. MacChesney, and C. M. Melliar-Smith, 1977, Electron. Lett. **13**, 170.
Okamoto, K., and T. Okoshi, 1976, IEEE Trans. Microwave Theory Tech. **MTT-24**, 416.
Okamoto, K., and T. Okoshi, 1977, IEEE Trans. Microwave Theory Tech. **MTT-25**, 213.
Olshansky, R., 1975a, Appl. Opt. **14**, 20.
Olshansky, R., 1975b, Appl. Opt. **14**, 935.
Olshansky, R., 1976a, Appl. Opt. **15**, 782.
Olshansky, R., 1976b, Appl. Opt. **15**, 2773.
Olshansky, R., 1976c, in *Proceedings of the Second European Conference on Optical Fibre Communication*, Paris (Comité du Colloque International sur le Transmission par Fibres Optiques, Paris), p. 101.
Olshansky, R., 1977a, Appl. Opt. **16**, 2171.
Olshansky, R., 1977b, (unpublished).
Olshansky, R., 1978, Electron. Lett. **14**, 330.
Olshansky, R., and D. B. Keck, 1976, Appl. Opt. **15**, 483.
Olshansky, R., and D. A. Nolan, 1976, Appl. Opt. **15**, 1045.
Olshansky, R., and D. A. Nolan, 1977, Appl. Opt. **16**, 1639.
Olshansky, R., S. M. Oaks, and D. B. Keck, 1977, in *Proceedings of the Topical Meeting on Optical Fiber Transmission II*, Williamsburg, Va., TuE5 (Optical Society of America, Washington, D.C.).
Onoda, S., T. Tanaka, and M. Sumi, 1976, Appl. Opt. **15**, 1931.
Osanai, H., T. Shioda, T. Moriyama, S. Araki, M. Horiguchi, T. Izawa, and H. Takata, 1976, Electron. Lett. **12**, 549.
Pask, C., A. W. Snyder, and D. J. Mitchell, 1975, J. Opt. Soc. Am. **65**, 356.
Payne, D. N., and W. A. Gambling, 1974, Electron. Lett. **10**, 289.
Payne, D. N., and A. H. Hartog, 1977, Electron. Lett. **13**, 627.
Payne, D. N., F. M. E. Sladen, and A. H. Hartog, 1978, Electron. Lett. **14**, 64.
Pearsall, T. P., 1978, in *Proceedings of the Fourth European Conference on Optical Communication*, Genoa (Instituto Internazionale delle Communicazioni, Genoa), p. 332.
Personick, S. D., 1971, Bell Syst. Tech. J. **50**, 843.
Personick, S. D., 1973, Bell Syst. Tech. J. **52**, 843.
Petermann, K., 1975, Archiv Elektron. Ubertragungstechnik. **29**, 345.
Petermann, K., 1976a, Electron. Lett. **12**, 107.
Petermann, K., 1976b, Archiv Elektron. Ubertragungstechnik. **30**, 337.
Petermann, K., 1977a, Archiv Elektron. Ubertragungstechnik. **31**, 201.
Petermann, K., 1977b, Electron. Lett. **13**, 513.
Petermann, K., and H. Storm, 1976, Electron. Lett. **12**, 537.
Pinnow, D. A., T. C. Rich, F. W. Ostermayer, Jr., and M. DiDomenico, Jr., 1973, Appl. Phys. Lett. **22**, 527.
Pinnow, D. A., L. G. Van Uitert, T. C. Rich, F. W. Ostermayer, and W. H. Grokiewicz, 1975, in *Proceedings of the Topical Meeting on Optical Fiber Transmission*, Williamsburg, Va., TuA3 (Optical Society of America, Washington, D.C.).
Presby, H. M., and I. P. Kaminow, 1976, Appl. Opt. **15**, 3029.
Roberts, R., 1975, Electron Lett. **11**, 529.
Rowe, H. E., and D. T. Young, 1972, IEEE Trans. Microwave Theory Tech. **MTT-20**, 349.
Runk, R. B., 1977, in *Proceedings of the Topical Conference on Optical Fiber Transmission II*, Williamsburg, Va., TuB5 (Optical Society of America, Washington, D.C.).
Sammut, R. A., 1977, Electron. Lett. **13**, 418.
Schroeder, J., R. Mohr, P. B. Macedo, and C. J. Montrose, 1973, J. Am. Ceram. Soc. **56**, 510.
Schultz, P. C., 1973, American Ceramic Society meeting, Cincinnati, Ohio.
Schultz, P. C., 1974, J. Am. Ceram. Soc. **57**, 360.
Schultz, P. C., 1977, in *Proceedings of the XIth International Congress on Glass*, Prague, published in J. Non-Cryst. Solids **25**, 26.
Schultz, P. C., 1979, in *Proceedings of the Conference on Physics of Fiber Optics*, edited by S. S. Mitra and B. Bendow (Plenum, New York).
Shen, C. C., J. J. Hsieh, and T. A. Lind, 1977, Appl. Phys. Lett. **30**, 353.
Shevchenko, V. V., 1973, Radiophys. Quant. Electron. **14**, 607.
Sladen, F. M. E., D. N. Payne, and M. J. Adams, 1975, Appl. Phys. Lett. **28**, 255.
Sladen, F. M. E., D. N. Payne, and M. J. Adams, 1977, Electron. Lett. **13**, 212.
Sladen, F. M. E., D. N. Payne, and M. J. Adams, 1978, in *Proceedings of the Fourth European Conference on Optical Communication*, Genoa (Instituto Internazionale delle Communicazioni, Genoa), p. 48.
Snitzer, E., 1961, J. Opt. Soc. Am. **51**, 491.
Snyder, A. W., 1969, IEEE Trans. Microwave Theory Tech. **MTT-17**, 1130.
Snyder, A. W., 1970, IEEE Trans. Microwave Theory Tech. **MTT-18**, 323.
Snyder, A. W., 1971, IEEE Trans. Microwave Theory Tech. **MTT-19**, 402.
Snyder, A. W., and J. D. Love, 1976a, Electron. Lett. **12**, 255.
Snyder, A. W., and J. D. Love, 1976b, Electron. Lett. **12**, 325.
Snyder, A. W., and D. J. Mitchell, 1974, J. Opt. Soc. Am. **64**, 599.
Snyder, A. W., D. J. Mitchell, and C. Pask, 1974, J. Opt. Soc. Am. **64**, 608.
Snyder, A. W., I. White, and D. J. Mitchell, 1975, Electron. Lett. **11**, 332.
Sommer, R. G., R. D. DeLuca, and G. E. Burke, 1976, Electron. Lett. **12**, 408.
Spitzer, W. G., and D. A. Kleinman, 1961, Phys. Rev. **121**, 1324.
Stacey, K. A., 1956, *Light Scattering in Physical Chemistry* (Academic, New York), p. 8.
Stewart, W. J., 1975a, in *Proceedings of the Topical Meeting on Optical Fiber Transmission*, Williamsburg, Va. (Optical Society of America, Washington, D. C.).
Stewart, W. J., 1975b, Electron. Lett. **11**, 321.
Streifer, W., and C. N. Kurtz, 1967, J. Opt. Soc. Am. **57**, 779.
Tanaka, T., S. Onada, and M. Sumi, 1976, Appl. Opt. **15**, 1121.
Tasker, G. W., W. G. French, J. R. Simpson, P. Kaiser, and H. M. Presby, 1978, Appl. Opt. **17**, 1836.
Tauc, J., 1975, in *Optical Properties of Highly Transparent Solids*, edited by S. S. Mitra and B. Bendow (Plenum, New York).
Tenney, A. S., and J. Wong, 1972, J. Chem. Phys. **56**, 5516.
Timmermann, C. C., 1977, Appl. Opt. **16**, 1793.
Tusuchiya, J., and I. Hayakayama, 1977, in *Proceedings of the Topical Meeting on Optical Fiber Transmission II*, Williamsburg, Va., PD1-1 (Optical Society of America, Washington, D.C.).
Tynes, A. R., and R. M. Derosier, 1977, Electron. Lett. **13**, 673.
Uchida, N., N. Susa, and S. Seikai, 1978, Electron. Lett. **14**, 80.
Uchida, T., M. Furukawa, I. Kitano, K. Koizumi, and H. Matsumura, 1970, IEEE J. Quant. Electron. **QE-6**, 606.
Unger, H.-G., 1977, *Planar Optical Waveguides and Fibres* (Clarendon, Oxford).
Urbach, F., 1953, Phys. Rev. **92**, 1324.
Wemple, S. H., D. A. Pinnow, T. C. Rich, R. E. Jaeger, and L. G. Van Uitert, 1973, J. Appl. Phys. **44**, 5432.
Wong, J., 1976, J. Non-Cryst. Solids **20**, 83.
Yamauchi, R., T. Kobayashi, T. Arai, and K. Inada, 1977, Electron. Lett. **13**, 461.
Yoshida, K., Y. Furui, S. Sentsui, and T. Kuroha, 1977, Electron. Lett. **13**, 608.
Yoshida, K., S. Sentsui, H. Shii, and T. Kuroha, 1977, in *Proceedings of the International Conference on Integrated Optics and Optical Fiber Communication*, Tokyo (Institute of Electronics and Communication Engineers of Japan, Tokyo), p. 327.
Zemon, S., and D. Fellows, 1976, Appl. Opt. **15**, 1937.